Faculty of Fundamental Problems of Technology
Wrocław University of Science and Technology

Eigenmodes in nearly integrable quantum chains

Jakub Pawłowski
Index number: 250193

Master thesis
under supervision of
prof. dr hab. Marcin Mierzejewski

Wrocław
University
of Science
and Technology

Wrocław 2023

This page is intentionally left blank.

I

This page is intentionally left blank.

Abstract

A

Keywords: *integrals of motion, ETH, nearly integrable systems, spin chains*

This page is intentionally left blank.

Contents

This page is intentionally left blank.

1 Introduction

1.1 Nearly integrable quantum systems

One of the most widely disputed problems in modern physics is the reconciliation of irreversible thermodynamics [1, 2] with unitary, time-reversible dynamics predicted by quantum mechanics [3, 4]. In other words, it is the question of whether a generic, isolated quantum system can and will 'forget' about its initial, nonequilibrium state. In recent years, this problem has attracted the attention of many physicists, especially taking into account experimental evidence of the loss of information, or thermalization, in isolated systems [5–9]. Understanding this phenomenon is a crucial first step to controlling it, and perhaps to the creation of sought-after, robust systems which do not exhibit such behavior. After all, 'forgetting' about the initial state is equivalent to scrambling of quantum information and decoherence, which has been known for a long time to be one of the most important hindrances to a functional and scalable quantum computer [10, 11]. Given the multitude of possible applications of such a device, both purely scientific and commercial, controlling thermalization in isolated systems could be the next groundbreaking achievement [12].

Preventing thermalization A possible theoretical explanation of the thermalization in isolated quantum systems has been proposed in seminal papers by Deutsch [13] and Srednicki [14] in form of an ansatz for matrix elements of local quantum observables $A_{mn} = \langle m|A|n\rangle$ (in eigenbasis $H|n\rangle = \varepsilon_n|n\rangle$ of some Hamiltonian), known as **Eigenstate Thermalization Hypothesis** (ETH)

$$A_{mn} = A(\bar{\varepsilon})\delta_{mn} + \mathrm{e}^{-S(\bar{\varepsilon})/2} f_A(\bar{\varepsilon}, \omega) R_{mn} \tag{1.1}$$

where $\bar{\varepsilon} = (\varepsilon_n + \varepsilon_m)/2$, $\omega = \varepsilon_n - \varepsilon_m$ and $S(\bar{\varepsilon})$ is the thermodynamic entropy at energy $\bar{\varepsilon}$, $A(\bar{\varepsilon})$ and $f_A(\bar{\varepsilon}, \omega)$ are some smooth functions of their parameters and R_{mn} is a random real or complex variable. The origin of ETH is the Random Matrix Theory [15, 16], but it was the key insight of Deutsch and Srednicki that connected it directly to statistical mechanics. Unraveling the physics behind equation (1.1), we have that, for generic systems, long-time (thermalized) expected values of local observables are related to the predictions of Gibbsian ensembles known

from equilibrium statistical physics [17]. Diagonal matrix elements $A_{nn} \simeq A(\varepsilon_n)$ are smooth functions of energy and coincide with the microcanonical average at energy ε_n, whereas the off-diagonal matrix elements and fluctuations of the diagonal ones are postulated to decrease exponentially with system size [18]. While ETH has been shown to hold analytically in only a few selected systems [19], numerical clues can be found in various systems with many-body interactions such as hard-core bosons, interacting spin chains [20–23] and fermions [24, 25].

Given the lack of a definitive answer to the question of when ETH holds and the fact that our ultimate goal is preventing thermalization, it is desirable to look for systems that explicitly violate this hypothesis. There are a few known classes of such systems: quantum integrable models, systems with 'scars', which freeze thermalization for some infrequent, but physically relevant states [26, 27], quantum time crystals with broken time-translation symmetry [28, 29] and systems with many-body interactions together with some form of disorder [30]. As the thermalization in those systems is slowed down or even completely stopped, in principle they could preserve information about the initial state for an arbitrarily long time. This behavior is in stark contrast with what is usually observed in interacting, many-body systems, namely fast dynamics on the time scales of tens of femtoseconds [31]. In this thesis, we shall concern ourselves only with the case of **quantum integrable models**.

Robustness of integrability In quantum mechanics, as opposed to classical mechanics, a unique definition of integrability is yet to emerge [32, 33]. Nevertheless, a common practice is to take as a sufficient condition of integrability the presence of an extensive number (increasing linearly with the system size) of local observables that are integrals of motion, i.e. commute with the Hamiltonian, called LIOMs for short. The significance of such systems is at least twofold. First, as already mentioned, they can provide a new method of storage of information, encoded in expectation values of LIOMs, which can pave the way for the creation of the sought-after quantum memory. Second, they are among a few quantum many-body systems that are susceptible to analytical methods and so provide a rich playground for both theoretical physicists and mathematicians. Tools such as Algebraic Bethe Ansatz [34–36] or Generalized Hydrodynamics [37–41] lead to considerable insight regarding the nature of integrable systems.

Unfortunately, it is often the case for integrable systems such as Heisenberg, Hubbard or Lieb-Linger models whose integrability relies on a certain set of fine-tuned parameters. Any deviation from these parameters, eg. in the form of some perturbation, can very easily destroy the integrability. Exactly this situation takes place in most experimental setups (albeit some signatures of integrability were observed [42], suggesting sufficient proximity to an integrable system), even though the capabilities and precision of control have reached remarkable levels [43]. Therefore, **more realistic systems are expected to be described by nearly integrable systems**, containing some non-negligible perturbations that impact integrability [44, 45]. This renders all the formalism for investigations of purely integrable systems inapplicable and forces one to rely mostly on numerical methods (for a recent review see Bertini et al. [39]). A general expectation for such nearly integrable systems is such, that in the thermodynamic limit, an arbitrarily small perturbation should restore generic chaotic dynamics, which leads to thermalization [46]. However, there are some reports about surviving traces of integrability, for example in the form of residual quasiconserved quantities [45]. In

most cases numerical methods can only access finite systems and indirect transitions to infinite system sizes, such as finite-size scaling, pose great difficulties when executed properly, eg. first thermodynamic limit and then infinite time limit [47, 48]. Therefore, it is important to first gain a deep understanding of **weakly-perturbed finite systems**. Such endeavor immediately raises a few questions: How strong should a perturbation in a finite systems be to destroy integrability and how to efficiently describe resulting slow dynamics? Recently, those and other similar questions have been asked concerning the phenomena of ergodicity breaking phase transitions [49, 50]. Insight from experiments with ultracold atomic gases suggest also another way for nearly integrable systems to emerge, namely generic, chaotic one- and quasi-one-dimensional systems that exhibit approximately integrable dynamics on experimentally relevant timescales, because of a lack of rapid local thermalization [51, 52].

In classical mechanics, answers to those types of questions are given by the Hamiltonian perturbation theory [53]. There, the distinction between integrable and non-integrable systems is well understood. It is known, that for classical systems with n degrees of freedom to be integrable, it is sufficient to have n integrals of motion $\{H, F_i\} = 0$, $i \in \{1, \ldots, n\}$ that are in involution, i.e. $\{F_i, F_j\} = 0$ for any $i, j \in \{1, \ldots, n\}$. Then, dynamics are restricted to an n-dimensional torus in the phase space. The fate of such invariant tori under integrability-breaking perturbations is given by the famous Kolmogorov-Arnold-Moser theorem (KAM) [54–56], stating that for systems with finite degrees of freedom, majority of the invariant tori occupying the phase space survive the influence of small perturbations. However, as of now, there is no equivalent of this result in quantum mechanics. Nevertheless, such quantum systems are very intriguing as they can facilitate robust prethermalization plateaux, i.e. dynamics that at intermediate times resemble that of integrable models (at least for suitably weak perturbations), even though the system eventually thermalizes at longer times [57–60].

1.2 Motivation and aim of this dissertation

As argued in the previous section, nearly integrable quantum systems constitute an important relaxation of constraints imposed on ordinary integrable systems, facilitating experimental realizations. They form the broader context this thesis is set in and the main motivation. However, to keep it finite in size, we restrict our attention to two concrete problems.

First, we provide a pedagogical introduction to the so-called **Krylov subspace methods** which allow us to leverage the sparsity of local observables in order to avoid the limitations originating from the exponential growth of many-body Hilbert space. Following the exposition by Trefethen and Bau [61], in Chapter 2 we start our journey seemingly far away from physics, investigating a general algorithm called Arnoldi iteration, which original aim was to reduce a matrix to 'almost triangular' or Hessenberg form. Along the way we discover that, as a byproduct, Arnoldi iteration produces a remarkably good approximation of extremal eigenvalues and eigenvectors. Contrary to most physics texts and in the spirit of the pedagogical nature of this chapter, we try to derive all results when possible and motivate them thoroughly when not. Setting course back to physics, next, we assume that our matrices are Hermitian and observe how the Arnoldi iteration simplifies tremendously, producing the well known

Lanczos iteration [62]. Then, going beyond just groundstate calculations, we show how to slightly modify Lanczos iteration to be able to compute an approximation of action of any analytic function of hermitian matrix on a vector. Applying this scheme to the function $f(x) = \exp(-ixt)$, we obtain an efficient way of calculating pure state time evolution, called the Krylov propagator [63]. At the end of Chapter 2, we outline the recent concept of Quantum Typicality [64] and derive a numerical procedure for efficient calculation of correlation functions, without the need for Exact Diagonalization. All algorithms described in chapter 2 were implemented using the Armadillo linear algebra library [65] and Intel MKL.

Go back to this part after finishing chapters on physics, add some citations Our second topic of interest is the **spin transport in the long-range anisotropic Heisenberg model.** Existence of many interesting features of quantum many-body systems, such as ballistic dynamics in Heisenberg spin chains [39, 66], exotic frustrated magnetism [67], peculiar phase transitions [68, 69] and entangled spin liquids [70] depends strongly on the type and range of interaction present in them, so it is safe to say that it plays a crucial role. In the last few years, considerable development of experimental techniques has occurred, allowing for unprecedented manipulation of the interactions. Platforms such as individually controlled Rydberg atoms, or optical lattices provide insight into the properties of quantum many-body systems. Whereas optical lattice facilitates mostly fermionic systems [71–74], Rydberg atoms can be used to simulate pure spin systems. Models such as Ising or XY emerge naturally from their properties [43], and the ability to control range of interactions make them suitable for the simulation of long-range models [75]. Using time-periodic driving one can turn naturally existing Hamiltonian into some other, effective one - the so-called Floquet Hamiltonian. So far, this method has been applied with great success to create tunable XXZ model [76], strongly distance selective interactions [77], and tunable XYZ models [78, 79]. Progress in experimental methods sparked theoretical interest in long-range models [80–91], yet their dynamical properties are still largely unknown, which explains our interest in long-range anisotropic Heisenberg model in this thesis. In Chapter 3, motivated by experiments with density expansion in cold atoms [92–94], we study the dynamics of spin domains using the Krylov propagator, followed by Exact Diagonalization studies of the optical conductivity. Chapter 4 is devoted to investigating a class of local observables exhibiting similar properties to the spin current, using a numerical procedure searching for most conserved operators [95]. It is worth noting that the results presented in Chapters 3 and 4 have been recently published in Mierzejewski et al. [96].

The remainder of this chapter is devoted to the short introduction to the long-range anisotropic Heisenberg model and other quantities of interest.

1.3 Long range anisotropic Heisenberg model and spin current

In this thesis, we study the paradigmatic quantum model of magnetism, the anisotropic Heisenberg model, but enriched with a long-range exchange $J(r) = J/r^{\alpha}$. The full Hamiltonian,

defined on a one-dimensional lattice with periodic boundary conditions, reads

$$H = \sum_{\ell=1}^{L} \sum_{r=1}^{r_{\max}} J(r) \left[\frac{1}{2} \left(S_\ell^+ S_{\ell+r}^- + S_\ell^- S_{\ell+r}^+ \right) + \Delta S_\ell^z S_{\ell+r}^z \right] \tag{1.2}$$

where $r_{\max}$ is taken to be $\lceil L/2 \rceil - 1$, to avoid double counting of hoppings. Unless stated otherwise, we will work in units where $J = 1$. The spin$-\frac{1}{2}$ operators are defined in the usual way

$$S_\ell^a = \underbrace{\mathbb{1} \otimes \mathbb{1} \otimes \ldots \mathbb{1}}_{\ell-1} \otimes S^a \otimes \underbrace{\mathbb{1} \otimes \ldots \otimes \mathbb{1}}_{L-\ell} \tag{1.3}$$

where $a \in \{+, -, z\}$, $S^+ = S^x + iS^y$, $S^- = \left(S^+\right)^\dagger$, $\mathbb{1}$ is a 2×2 identity matrix and operators S^x, S^y, S^z are defined in terms of corresponding Pauli matrices and obey the $\mathfrak{su}(2)$ algebra commutations relations

$$\left[S^a, S^b \right] = i\varepsilon_{abc} S^c \tag{1.4}$$

From equation (1.3) it is evident, that the Hilbert space $\mathcal{H}$ our Hamiltonian acts on is the tensor product of L copies of single spin spaces $\mathfrak{h}_\ell \cong \mathbb{C}^2$,

$$\mathcal{H} = \bigotimes_{\ell=1}^{L} \mathfrak{h}_\ell \tag{1.5}$$

As $\dim_{\mathbb{C}}(\mathfrak{h}) = 2$, the total dimension is 2^L. For numerical calculations, we shall use the so-called **Ising basis**, consisting of eigenstates of the $S_{\text{tot}}^z = \sum_{\ell=1}^{L} S_\ell^z$ operator. As on each site we can only have spin up or down, an efficient representation of such states is achieved using binary numbers.

Our main interest is in the spin transport in this system. To this end, we first notice that the total magnetization, or z component of the total spin S_{tot}^z is a conserved quantity. It can be shown by directly evaluating the commutator $[H, S_{\text{tot}}^z] = 0$, or by just observing that both spin-flip and interaction terms do not change the number of up/down spins when acting on a state from the Ising basis. Thus, we can write down a well-defined continuity equation for the evolution of local spin density

$$\frac{\mathrm{d}}{\mathrm{d}t} S_\ell^z(t) + \boldsymbol{\nabla} \cdot j_\ell^\sigma(t) = 0 \tag{1.6}$$

where $\boldsymbol{\nabla} \cdot j_\ell^\sigma(t) = j_{\ell+1}^\sigma(t) - j_\ell^\sigma$ is the discrete divergence of the spin current and $S_\ell^z(t) = e^{iHt} S_\ell^z e^{-iHt}$. The time derivative in the above equation is given by the Heisenberg equation

$$\frac{\mathrm{d}}{\mathrm{d}t} S_\ell^z(t) = i[H, S_\ell^z(t)] \tag{1.7}$$

Combining equations (1.6) and (1.7), we get

$$j_{\ell+1}^\sigma - j_\ell^\sigma = i[S_\ell^z, H] \tag{1.8}$$

This equation is simple in principle, however, its solution can get tedious in case of more complicated operator densities.

Fortunately, there is a trick that yields a simple expression for the current associated with an arbitrary conserved, extensive operator. Let $X = \sum_{\ell=1}^{L} x_l$ be such quantity, with x_ℓ being its local density and $j^x = \sum_{\ell=1}^{L} j_\ell^x$ being the current. Then define the polarization operator

$$P = \sum_{\ell=1}^{L} \ell x_\ell \tag{1.9}$$

We will now calculate its derivative in two ways, first using the continuity equation and second using the Heisenberg picture. For brevity, we suppress the explicit time dependence of operators.

$$\frac{\mathrm{d}P}{\mathrm{d}t} = \sum_{\ell=1}^{L} \ell \frac{\mathrm{d}x_\ell}{\mathrm{d}t} = \sum_{\ell=1}^{L} \ell j_\ell^x - \underbrace{\sum_{\ell=1}^{L} \ell j_{\ell+1}^x}_{\ell \to \ell-1} = \sum_{\ell=1}^{L} \left[\ell j_\ell^x - (\ell-1)\, j_\ell^x\right] = \sum_{\ell=1}^{L} j_\ell^x = j^x \tag{1.10}$$

$$\frac{\mathrm{d}P}{\mathrm{d}t} = \frac{\mathrm{d}}{\mathrm{d}t} \sum_{\ell=1}^{L} \ell \left(e^{iHt} x_\ell e^{-iHt}\right) = \sum_{\ell}^{L} \left(\ell e^{iHt} i[H, x_\ell] e^{-iHt}\right) = e^{iHt} \left(i \sum_{\ell} \ell [H, x_\ell]\right) e^{-iHt} \tag{1.11}$$

From the two equations above we can read off a compact expression for the current operator in Schrödinger picture

$$j^x = i \sum_{\ell=1}^{L} \ell [H, x_\ell] \tag{1.12}$$

Substituting $x_\ell = S_\ell^z$ we now quickly derive

$$\begin{aligned} j^\sigma &= i \sum_{\ell=1}^{L} [H, S_\ell^z] = i \sum_{\ell,\ell'=1}^{L} \sum_{r=1}^{r_{\max}} \ell J(r) \left(\frac{1}{2}\left[S_{\ell'}^+ S_{\ell'+r}^-, S_\ell^z\right] + \frac{1}{2}\left[S_{\ell'}^- S_{\ell'+r}^+, S_\ell^z\right] + \Delta \cancel{\left[S_{\ell'}^z S_{\ell'+1}^z, S_\ell^z\right]}\right) \\ &= \frac{i}{2} \sum_{\ell,\ell'=1}^{L} \sum_{r=1}^{r_{\max}} \ell J(r) \left(\delta_{\ell,\ell'+r} S_{\ell'}^+ S_{\ell'+r}^- - \delta_{\ell,\ell'} S_\ell^+ S_{\ell'+r}^- - \delta_{\ell'+r,\ell} S_{\ell'}^- S_\ell^+ + \delta_{\ell',\ell} S_\ell^- S_{\ell'+r}^+\right) \\ &= \frac{i}{2} \sum_{\ell'=1}^{L} \sum_{r=1}^{r_{\max}} J(r) \left((\ell'+r) S_{\ell'}^+ S_{\ell'+r}^- - \ell' S_{\ell'}^+ S_{\ell'+r}^- - (\ell'+r) S_{\ell'}^- S_{\ell'}^+ + \ell' S_{\ell'}^- S_{\ell'+r}^+\right) \\ &= \frac{i}{2} \sum_{\ell=1}^{L} \sum_{r=1}^{r_{\max}} \frac{J}{r^{\alpha-1}} \left(S_\ell^+ S_{\ell+r}^- - S_\ell^- S_{\ell+r}^+\right) \end{aligned} \tag{1.13}$$

which is our desired spin current. It will be the quantity of central interest in Chapter 3.

Before we finish the introductory chapter, let us notice two symmetries shared by the Hamiltonian (1.2) and spin current (1.13), which are particularly useful for numerical calculations. First of them we have just met – it manifests itself as the conservation of magnetization, i.e. $[H, S_{\mathrm{tot}}^z] = 0$. This $U(1)$ symmetry allows us to decompose the full Hilbert space into parts consisting of states with the same total z-component of spin. In more mathematical terms, we have the following

$$\mathcal{H} = \bigoplus_{j=0}^{L} \mathcal{H}_j, \text{ where } (\forall\, |\psi\rangle \in \mathcal{H}_j)(S_{tot}^z\, |\psi\rangle = \frac{1}{2}(2j - L)\, |\psi\rangle\,)$$

i.e., the full Hilbert space with $\dim \mathcal{H} = 2^L$ can be decomposed into the direct sum of its proper subspaces $\mathcal{H}_j$ such that $\dim \mathcal{H}_j = \binom{L}{j}$ and all states in a given subspace correspond to the same eigenvalue of S_{tot}^z operator. The index j denotes the number of sites with spin up. It turns out that the Ising basis we use as a default for numerical calculations in spin systems is already the 'correct' basis, as it is enough to just sort the states according to the number of spins pointing up. This yields a manifestly block diagonal structure of the Hamiltonian matrix (cf. Figure 2.2 with a matrix of nearest neighbors Heisenberg model).

Because we have assumed periodic boundary conditions, both the Hamiltonian and the spin current are invariant under translations by any number of sites - that is under the action

of $\mathbb{Z}_L$ cyclic group. This symmetry allows us to further decompose the Hilbert space using the eigenbasis of T, the one-site translation operator defined on the Ising basis as

$$T\,|\sigma_1, \sigma_2, \ldots, \sigma_L\rangle = |\sigma_L, \sigma_1, \ldots, \sigma_{L-1}\rangle \tag{1.14}$$

where $\sigma_\ell \in \{\downarrow, \uparrow\}$. It is easy to see that T is unitary, thus its eigenvalues must lie on the unit circle in the complex plane [97]. In a finite chain of length L we have $T^L = \mathbb{1}$ and the eigenvalues of T are quantized, i.e. of the form e^{ik}, where $k \in \left\{0, \frac{2\pi}{L}, \ldots, \frac{2\pi}{L}(L-1)\right\}$. As a consequence, the Hilbert space can be decomposed into the direct sum of eigenspaces of T

$$\mathcal{H} = \bigoplus_{m=0}^{L-1} \mathcal{H}_m, \text{ where } (\forall\,|\psi\rangle \in \mathcal{H}_m)(T\,|\psi\rangle = \exp\left(i\frac{2\pi}{L}m\right)|\psi\rangle\,) \tag{1.15}$$

and once again the Hamiltonian and the spin current are block diagonal in this basis, which each block being about L times smaller than the full Hilbert space. The practical construction of the momentum states is more complicated than that of the magnetization states, so it has been moved to Appendix A. Importantly, we also have $[T, S^z_{\mathrm{tot}}] = 0$ and thus the two symmetries are compatible. Using both of them at the same time, the size of the largest block is reduced to $\binom{L}{L/2}\frac{1}{L}$, which is still exponentially large in L, but much smaller than the full Hilbert space of dimension 2^L.

To end this chapter we note that these two symmetries are not the only ones present in this model. For a comprehensive treatment of this topic, together with details of numerical implementation, we refer the reader to Sandvik [62].

2

Krylov subspace methods for quantum many-body systems

One of the two purposes of this thesis is to develop and test a set of numerical tools based on the Krylov subspace methods, which is a family of **iterative** methods concerned with projecting high dimensional problems into smaller dimension subspaces and solving them therein. Given a finite-dimensional vector space $\mathcal{H} \cong \mathbb{C}^m$, a vector $\mathbf{v} \in \mathbb{C}^m$ and a linear operator $A \in \mathbb{C}^{m\times m}$, represented as a matrix, the **k-th Krylov subspace** $\mathcal{K}_k$ is defined as

$$\mathcal{K}_k := \text{span}\{\, \mathbf{v}, A\mathbf{v}, A^2\mathbf{v}, \ldots, A^{k-1}\mathbf{v} \,\} \subseteq \mathbb{C}^m \tag{2.1}$$

The maximal dimension of a Krylov subspace is bounded from above by $\text{rank}(A) + 1$ [98].

This chapter serves as a pedagogical introduction to the core ideas of these methods, including some of the usually omitted mathematical details. For the initial part of this exposition, we follow the excellent textbook of numerical linear algebra by Trefethen and Bau [61], whereas for further applications to quantum many-body physics, we rely on the excellent treatments of the topic found in Sandvik [62] and PhD thesis by Crivelli [99].

We start this chapter by quickly sketching the problems with **direct** algorithms such as Exact Diagonalization (ED), and quickly follow with the fundamental iterative algorithm for sparse general matrices, the Arnoldi iteration. Its output admits several possible interpretations, however, we shall focus on the problem of locating extremal eigenvalues. Afterward, we restrict our attention to the class of Hermitian matrices, to which of course all typical tight-binding Hamiltonians belong to, and describe the Lanczos algorithm, which allows for efficient calculation of the ground state eigenvalue and eigenvector, and thus the ground state properties of a system. Yet in this work, we are mainly interested in infinite temperature calculations, for which in principle sampling of the whole spectrum is required. To this end, in subsequent sections, we develop a scheme for the time evolution of an arbitrary state, called the Krylov propagator [63], and in the last section combine it with the idea of Dynamical Quantum Typicality (DQT), which states that a single pure state can have the same properties as an ensemble density matrix [100–102]. This will produce a numerical algorithm for the efficient calculation of time-dependent correlation functions without the need for Exact Diagonalization.

2.1 Problems with Exact Diagonalization

The most straightforward numerical method for studying discrete quantum many-body systems is without a doubt Exact Diagonalization (ED) [103]. It belongs to the family of the so-called direct algorithms (cf. Fig 2.1) and allows one to obtain a numerically exact set of eigenvalues and eigenvectors and subsequently compute any desired properties of the system, be it thermal expectation values, time evolution, Green's functions, etc. Unfortunately, the starting point of any ED calculation is the expression of the Hamiltonian as a dense matrix, in the Hilbert space basis of choice. Taking into account the fact that the dimension many-body Hilbert space grows exponentially with the size of the system, the memory cost quickly becomes prohibitive, even when exploiting conservation laws and related symmetries. For example, in the case of a spin chain of length L, with the on-site basis dimension being 2, the full dimension of the Hilbert space would be $\mathcal{D} = 2^L$. Taking a modest length of 25 sites gives $2^{25} = 33554432 \approx 3.36 \cdot 10^7$ basis states and a memory footprint of the Hamiltonian matrix of around 9PB (using double-precision floating point numbers), which is 9000 times more than the typical consumer hard drive capacity of 1TB. Even assuming some kind of distributed memory platform allowing for handling such large matrices, the computational complexity of ED, requiring $O(\mathcal{D}^3)$ operations, is the next major hurdle. Therefore, it is exceedingly difficult to probe the thermodynamic limit physics and ED calculations suffer from finite size effects.

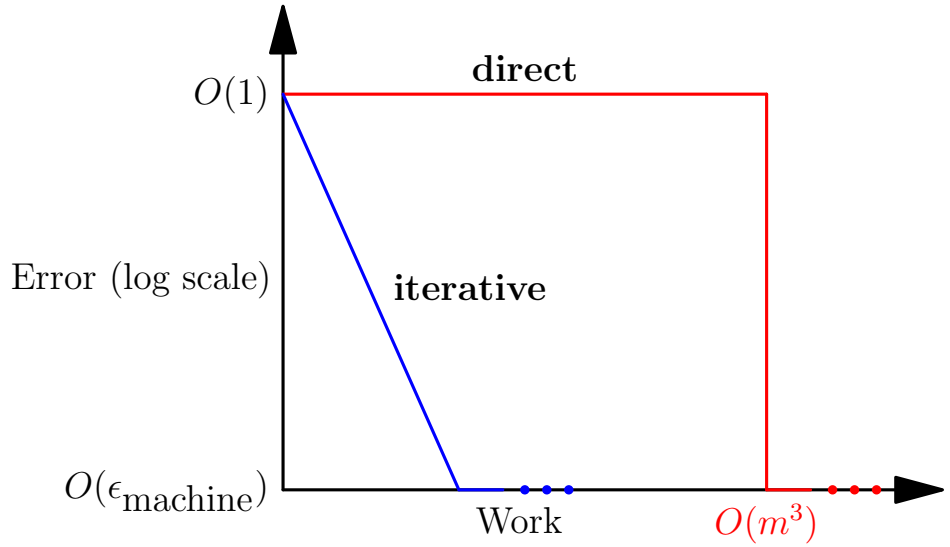

Figure 2.1: Schematic representation of the difference between direct (such as Exact Diagonalization) and iterative (such as Lanczos iteration) algorithms. The advantage of iterative methods comes from the fact that they can be stopped midway after desired precision is reached. On the other hand, direct algorithms require all $O(m^3)$ operations before any results can be extracted. Figure reproduced from Trefethen and Bau [61].

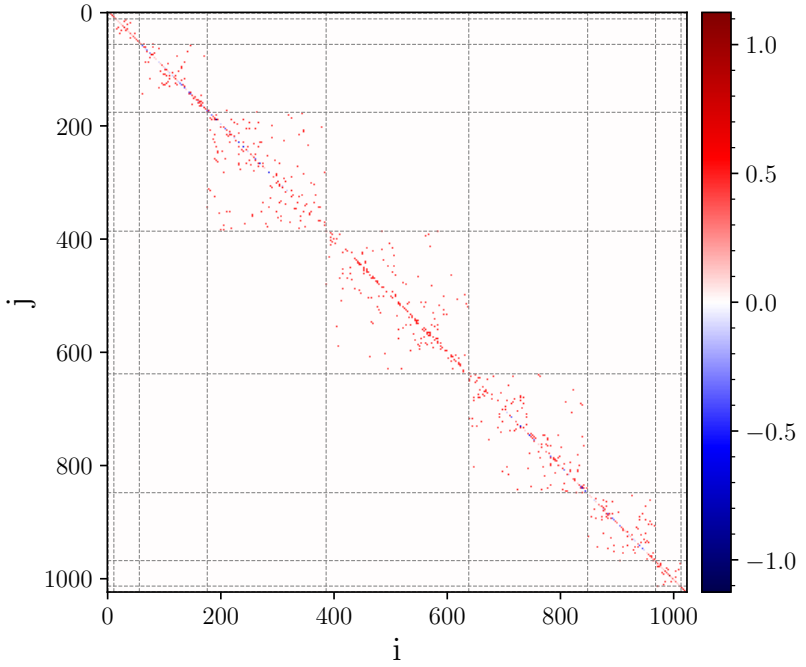

Figure 2.2: Ising basis representation of matrix of the XXZ Hamiltonian $H = J\sum_i \left[\frac{1}{2}\left(S_i^+ S_{i+1}^- + S_i^- S_{i+1}^+\right) + \Delta S_i^z S_{i+1}^z\right]$ on 10 sites, with $J = 1$ and $\Delta = 0.5$. Basis states are sorted according to the magnetization which yields the block structure emphasized by dashed lines. The filling factor μ is approximately 0.005.

A closer investigation of the Hamiltonian matrix, expressed in the Ising basis, quickly reveals the inefficiency of dense storage. Looking at Figure 2.2, we see that most of the matrix elements are zero. Only about $\mu \propto \mathcal{D}$ out of $\mathcal{D}^2$ matrix elements are non-zero. Hence, a numerical scheme leveraging this sparsity is highly desirable. This is exactly what the Krylov subspace algorithms do, by the virtue of requiring only a "black box" computation of matrix-vector product, which can be fairly easily implemented in a way requiring only $O(\mu\mathcal{D})$ operations.

2.2 Calculation of ground state

Our goal in this section is to develop the Lanczos algorithm for ground-state search of Hermitian matrices, and along the way to understand how and why it works.

2.2.1 Arnoldi iteration

The Lanczos algorithm is a special case of a more general algorithm, called Arnoldi iteration, designed to transform a general, non-Hermitian matrix $A \in \mathbb{C}^{m\times m}$ via a orthogonal [1] similarity transformation to a Hessenberg form $A = QHQ^\dagger$. Such transformation always exists [104]. A square, $m \times m$ matrix H is said to be in **upper Hessenberg form** if $\forall i, j \in \{1, \ldots, n\} : i >$

[1] Orthogonal in this context means that $Q^\dagger Q = I_{m\times m}$

$j+1 \implies (A)_{i,j} = 0$. It is said to be in **lower Hessenberg form** if its transpose is in upper Hessenberg form. A Hessenberg matrix differs from a triangular one by one additional super- or subdiagonal. Such form is desirable because many numerical algorithms in linear algebra experience considerable speedup from leveraging the triangular structure of a matrix, and sometimes those benefits carry over to this almost-triangular case. A particularly important strength of the Arnoldi iteration is that it can be interrupted before completion (cf Fig. 2.1), thus producing only an approximation of the Hessenberg form in a situation where m is so large, that full computations are infeasible (eg. in quantum many-body physics).

Assume now that we can only compute the first $n < m$ columns of the equation $AQ = QH$. Let Q_n be the restriction of Q to n columns and let them be denoted by $\mathbf{q_1}, \mathbf{q_2}, \dots \mathbf{q_n} \in \mathbb{C}^m$. Denoting by $\tilde{H}_n$ the $(n+1) \times n$ upper left section of H, which is also a Hessenberg matrix, we can write down the following n-step approximation to the full decomposition

$$AQ_n = Q_{n+1}\tilde{H}_n \tag{2.2}$$

From this equation we can deduce an $n+1$ term recurrence relation for the column $\mathbf{q_{n+1}}$, however it is perhaps best illustrated with a simple example in the first place.

Example 2.1 *Let $A \in \mathbb{C}^{3\times 3}$, $AQ = QH$ be the Hessenberg decomposition and corresponding matrix elements be denoted by lowercase letters. We consider the approximation for $n = 2$, i.e. $AQ_2 = Q_3\tilde{H}_2$. On the right-hand side*

$$AQ_2 = \begin{bmatrix} a_{11} & a_{12} & a_{13} \\ a_{21} & a_{22} & a_{23} \\ a_{31} & a_{32} & a_{33} \end{bmatrix} \begin{bmatrix} q_{11} & q_{12} \\ q_{21} & q_{22} \\ q_{31} & q_{32} \end{bmatrix} = \begin{bmatrix} a_{11}q_{11} + a_{12}q_{21} + a_{13}q_{31} & a_{11}q_{12} + a_{12}q_{22} + a_{13}q_{32} \\ a_{21}q_{11} + a_{22}q_{21} + a_{23}q_{31} & a_{21}q_{12} + a_{22}q_{22} + a_{23}q_{32} \\ a_{31}q_{11} + a_{32}q_{21} + a_{33}q_{31} & a_{31}q_{12} + a_{32}q_{22} + a_{33}q_{32} \end{bmatrix}$$
$$= \begin{bmatrix} (A\mathbf{q_1})_1 & (A\mathbf{q_2})_1 \\ (A\mathbf{q_1})_2 & (A\mathbf{q_2})_2 \\ (A\mathbf{q_1})_3 & (A\mathbf{q_2})_3 \end{bmatrix}$$

On the left-hand side

$$Q_3H_2 = \begin{bmatrix} q_{11} & q_{12} & q_{13} \\ q_{21} & q_{22} & q_{23} \\ q_{31} & q_{32} & q_{33} \end{bmatrix} \begin{bmatrix} h_{11} & h_{12} \\ h_{21} & h_{22} \\ 0 & h_{32} \end{bmatrix} = \begin{bmatrix} q_{11}h_{11} + q_{12}h_{21} & q_{11}h_{12} + q_{12}h_{22} + q_{13}h_{32} \\ q_{21}h_{11} + q_{22}h_{21} & q_{21}h_{12} + q_{22}h_{22} + q_{23}h_{32} \\ q_{31}h_{11} + q_{32}h_{21} & q_{31}h_{12} + q_{32}h_{22} + q_{33}h_{32} \end{bmatrix}$$
$$= \begin{bmatrix} h_{11}(\mathbf{q_1})_1 + h_{21}(\mathbf{q_2})_1 & h_{12}(\mathbf{q_1})_1 + h_{22}(\mathbf{q_2})_1 + h_{32}(\mathbf{q_3})_1 \\ h_{11}(\mathbf{q_1})_2 + h_{21}(\mathbf{q_2})_2 & h_{12}(\mathbf{q_1})_2 + h_{22}(\mathbf{q_2})_2 + h_{32}(\mathbf{q_3})_2 \\ h_{11}(\mathbf{q_1})_3 + h_{21}(\mathbf{q_2})_3 & h_{12}(\mathbf{q_1})_3 + h_{22}(\mathbf{q_2})_3 + h_{32}(\mathbf{q_3})_3 \end{bmatrix}$$

From the above calculation and 2.2 we can read off two identities

$$A\mathbf{q_1} = h_{11}\mathbf{q_1} + h_{21}\mathbf{q_2}$$
$$A\mathbf{q_2} = h_{21}\mathbf{q_1} + h_{22}\mathbf{q_2} + h_{32}\mathbf{q_3}$$

Therefore we get, assuming $\mathbf{q_1}$ is known,

$$\mathbf{q_2} = \frac{A\mathbf{q_1} - h_{11}\mathbf{q_1}}{h_{21}}$$
$$\mathbf{q_3} = \frac{A\mathbf{q_2} - h_{21}\mathbf{q_1} - h_{22}\mathbf{q_2}}{h_{32}}$$

Generalizing the above example, we arrive at the desired $n+1$ term recurrence relation for $\mathbf{q_{n+1}}$

$$\mathbf{q_{n+1}} = \frac{A\mathbf{q_n} - \sum_{m=1}^{n} h_{mn}\mathbf{q_m}}{h_{n+1,n}} \tag{2.3}$$

We can now easily cast the above recurrence into a pseudocode algorithm:

Algorithm 1 Arnoldi iteration

Input: $\mathbf{v} \in \mathbb{C}^m$, $A \in \mathbb{C}^{m\times m}$, number of steps n

Output: columns of Q_n, matrix elements of H_n

1: $\mathbf{q_1} = \mathbf{v}/\|\mathbf{v}\|$ ▷ components of $\mathbf{v}$ are usually drawn from uniform distribution
2: **for** $i = 1 : n-1$ **do**
3: $\quad \mathbf{q} = A\mathbf{q_i}$
4: $\quad$ **for** $j = 1 : i$ **do**
5: $\quad\quad h_{ji} = \mathrm{cdot}(\mathbf{q_j}, \mathbf{q})$ ▷ cdot is the complex dot product on $\mathbb{C}^m$.
6: $\quad\quad \mathbf{q} = \mathbf{q} - h_{ji}\mathbf{q_j}$ ▷ In exact arithmetic, this ensures orthogonality.
7: $\quad$ **end for**
8: $\quad h_{i+1,i} = \|\mathbf{q}\|$
9: $\quad \mathbf{q_{i+1}} = \mathbf{q}/h_{i+1,i}$
10: **end for**

Step 9 of the Algorithm 1 may be questionable, as we are dividing by a norm of a vector, which after all can be equal to zero. However, in practical applications of Arnoldi iteration, it usually means that our calculations have converged and the iterations may be stopped.

Examining closely the Arnoldi iteration algorithm, we notice that it is essentially the Gram-Schmidt procedure applied to the vectors $\{\mathbf{v}, A\mathbf{v}, \ldots, A^{n-1}\mathbf{v}\}$ and hence the vectors $\{\mathbf{q_1}, \mathbf{q_2}, \ldots, \mathbf{q_n}\}$ form an orthonormal basis of the Krylov subspace $\mathcal{K}_n$. The orthonormality condition is concisely expressed by the fact that $Q_n^\dagger Q_{n+1}$ is the $n \times (n+1)$ identity matrix. Multiplying the left-hand side of equation (2.2) by $Q_n^\dagger$ we get

$$Q_n^\dagger A Q_n = \underbrace{Q_n^\dagger Q_{n+1}}_{\mathrm{Id}_{n\times(n+1)}} \tilde{H}_n = H_n \in \mathbb{C}^{n\times n} \tag{2.4}$$

where H_n is the Hessenberg matrix $\tilde{H}_n$ with its last row removed.

To understand the meaning of matrix H_n from the point of view of linear algebra, consider the following reasoning. Imagine we are given an endomorphism of the space $\mathbb{C}^m$, represented in the standard basis by a matrix A. We would like to restrict it to an endomorphism of the Krylov subspace $\mathcal{K}_n$, $n < m$. Of course, as $\mathbf{q} \in \mathcal{K}_n \implies \mathbf{q} \in \mathbb{C}^m$, we can calculate the action of A on a vector from Krylov subspace in a straightforward way. However, the resulting vector $A\mathbf{q}$ is not guaranteed to be an element of $\mathcal{K}_n$. We need to orthogonally project it back to the subspace. Such projection is realized by $Q_nQ_n^\dagger \in \mathbb{C}^{m\times m}$ and hence, with respect to the standard basis on $\mathbb{C}^m$, the desired restriction can be written as $Q_nQ_n^\dagger A$. Transforming it to the basis given by columns of Q_n we get $Q_n^{-1}\left(Q_nQ_n^\dagger A\right)Q_n = Q_n^\dagger A Q_n$. Thus, matrix H_n is the orthogonal projection of A to the subspace $\mathcal{K}_n$, represented in the basis $\{\mathbf{q_1}, \mathbf{q_2}, \ldots, \mathbf{q_n}\}$.

H_n is once again a square matrix, so we can talk about its eigenvalues $\{\theta_i\}_{i=1}^n$ in the usual fashion. These numbers are called the *Arnoldi eigenvalues estimates at step n*, or the *Ritz*

values with respect to $\mathcal{K}_n$. Given the interpretation above, we may suspect that they would be related to the eigenvalues of the original matrix A. Indeed, as we shall see in a moment, some of the Ritz values are extremally good approximations of some of the original eigenvalues.

2.2.2 Polynomial approximation and eigenvalues

By carrying out the Arnoldi iterations for successive steps, and at each step n (or at just some of the steps) calculating the eigenvalues of the Hessenberg matrix H_n, we are left with sequences of Ritz values. Some of them often converge rapidly to, what we reasonably assume, are eigenvalues of the original matrix A. However, in practice, the maximal accessible n is much smaller than m, so we cannot expect to find all eigenvalues. As it turns out, Arnoldi iteration typically finds extremal eigenvalues, which fortunately are those that we are interested in.

Before we will understand the details, let us introduce a different, seemingly unrelated problem of *polynomial approximation*. We can take any $\mathbf{q} \in \mathcal{K}_n$ and using the defining basis of Krylov subspace $\mathcal{K}_n$(Definition 2.1), expand is as

$$\begin{aligned}\mathbf{q} &= a_0\mathbf{v} + a_1A\mathbf{v} + a_2A^2\mathbf{v} + \ldots + a_{n-1}A^{n-1}\mathbf{v} \\ &= \left(a_0\mathbb{1} + a_1A + a_2A^2 + \ldots + a_{n-1}A^{n-1}\right)\mathbf{v}\end{aligned}$$

Utilizing the special structure of vectors from $\mathcal{K}_n$, we can define a polynomial $p(z) = a_0 + a_1z + a_2z^2 + \ldots + a_{n-1}z^{n-1}$, and concisely write our vector as $\mathbf{q} = p(A)\mathbf{v}$. As the vector $\mathbf{q}$ was arbitrary, we have established an isomorphism between the n-th Krylov subspace and the space of complex polynomials of maximal degree $n-1$. We are now ready to state the problem:

Arnoldi Approximation Problem

Given a matrix $A \in \mathbb{C}^{m\times m}$ and a vector $\mathbf{v} \in \mathbb{C}^m$, find
$p \in P^n := \{\, a_0 + a_1z + \ldots + a_{n-1}z^{n-1} + z^n \mid a_0, a_1, \ldots a_{n-1} \in \mathbb{C}\,\}$
such that $\|p(A)\mathbf{v}\|_2$ is minimized.

Remarkably, the Arnoldi approximation is the exact solution to this problem. This fact is interesting enough that we state it here as a theorem and, following Trefethen and Bau [61], provide a complete proof.

Theorem 2.1 *If* $\dim(\mathcal{K}_n) = n$, *i.e. matrix having columns* $\mathbf{v}, A\mathbf{v}, \ldots, A^{n-1}\mathbf{v}$ *is of rank* n, *then the Arnoldi Approximation Problem has a unique solution* $p^n \in P^n$, *given by the characteristic polynomial of the matrix* H_n, *defined by* (2.4).

Proof. We start with an observation, that given a polynomial $p \in P^n$, the vector $p(A)\mathbf{v}$ can be written as $p(A)\mathbf{v} = A^n\mathbf{v} - Q_n\mathbf{r}$ for some $\mathbf{r} \in \mathbb{C}^n$. To see that, note that $(A^n\mathbf{v} - p(A)\mathbf{v}) \in \mathcal{K}_n$ and columns of Q_n form an orthonormal basis of $\mathcal{K}_n$. Now, we can recast our problem into a slightly different language, namely finding a vector in $\mathcal{K}_n$ that is the closest in the sense of L_2 norm to $A^n\mathbf{v}$. In short:

$$\mathbf{r}^* = \min_{\mathbf{r}\in\mathbb{C}^n} \|A^n\mathbf{v} - Q_n\mathbf{r}\|$$

To achieve that, we need to have $p(A)\mathbf{v} \perp \mathcal{K}_n$, that is $p(A)\mathbf{v}$ must be orthogonal to all basis vectors spanning $\mathcal{K}_n$. This is consisely expressed as $Q_n^\dagger p(A)\mathbf{v} = \mathbf{0} \in \mathbb{C}^n$.

Now, we know that the Hessenberg factorization $A = QHQ^\dagger$ exists, and is approximated by n steps of the Arnoldi iteration. Thus, the matrices Q and H can have the following block structure:

$$Q = \begin{bmatrix} Q_n & V \end{bmatrix}, \quad H = \begin{bmatrix} H_n & 0_{n\times(m-n)} \\ Y & 0_{(m-n)\times(m-n)} \end{bmatrix} \tag{2.5}$$

where $V \in \mathbb{C}^{m\times(m-n)}$ is a matrix with orthonormal columns, which are also orthogonal to columns of Q_n, and matrix $Y \in \mathbb{C}^{(m-n)\times n}$ has only the upper-right entry different from zero (the one from the last row of $\tilde{H}_n$). Using the Hessenberg factorization we can write our condition as $Q_n^\dagger Q p(H) Q^\dagger \mathbf{v} = \mathbf{0}$, and because equation (2.5) introduces partitions into *conformable* blocks, we can use the rules of block-matrix algebra to simiplify it further [105].

First, let us investigate closely the structure of $p(H)$. We observe that

$$\begin{aligned}
H^2 &= \begin{bmatrix} H_n & 0_{n\times(m-n)} \\ Y & 0_{(m-n)\times(m-n)} \end{bmatrix}^2 = \begin{bmatrix} H_n^2 & 0_{n\times(m-n)} \\ YH_n & 0_{(m-n)\times(m-n)} \end{bmatrix} \\
H^3 &= \begin{bmatrix} H_n & 0_{n\times(m-n)} \\ Y & 0_{(m-n)\times(m-n)} \end{bmatrix}^3 = \begin{bmatrix} H_n^3 & 0_{n\times(m-n)} \\ YH_n^2 & 0_{(m-n)\times(m-n)} \end{bmatrix} \\
&\dots \\
H^n &= \begin{bmatrix} H_n & 0_{n\times(m-n)} \\ Y & 0_{(m-n)\times(m-n)} \end{bmatrix}^n = \begin{bmatrix} H_n^n & 0_{n\times(m-n)} \\ YH_n^{n-1} & 0_{(m-n)\times(m-n)} \end{bmatrix}
\end{aligned}$$

Thus $p(H)$ can be written as

$$\begin{aligned}
p(H) &= a_0\mathbb{1} + a_1 H + a_2 H^2 + \ldots + a_{n-1}H^{n-1} + H^n \\
&= \begin{bmatrix} a_0\mathbb{1} + a_1 H_n + a_2 H_n^2 + \ldots + a_{n-1}H_n^{n-1} + H_n^n & 0_{n\times(m-n)} \\ a_0\mathbb{1} + a_1 Y + a_2 Y H_n + \ldots + a_{n-1} Y H_n^{n-2} + Y H_n^{n-1} & 0_{(m-n)\times(m-n)} \end{bmatrix} \\
&= \begin{bmatrix} p(H_n) & 0 \\ \tilde{Y} & 0 \end{bmatrix}
\end{aligned}$$

We have now all the pieces to simplify the orthogonality condition:

$$\begin{aligned}
\mathbf{0} &= Q_n^\dagger Q p(H) Q^\dagger \mathbf{v} \\
&= \begin{bmatrix} Q_n^\dagger \end{bmatrix} \begin{bmatrix} Q_n & V \end{bmatrix} \begin{bmatrix} p(H_n) & 0_{n\times(m-n)} \\ \tilde{Y} & 0_{(m-n)\times(m-n)} \end{bmatrix} \begin{bmatrix} Q_n^\dagger \\ U^\dagger \end{bmatrix} \mathbf{v} \\
&= \begin{bmatrix} \mathbb{1}_{n\times n} & 0_{n\times(m-n)} \end{bmatrix} \begin{bmatrix} p(H_n) & 0_{n\times(m-n)} \\ \tilde{Y} & 0_{(m-n)\times(m-n)} \end{bmatrix} \begin{bmatrix} Q_n^\dagger \\ U^\dagger \end{bmatrix} \mathbf{v} \\
&= \begin{bmatrix} p(H_n) & 0_{n\times(m-n)} \end{bmatrix} \begin{bmatrix} Q_n^\dagger \\ U^\dagger \end{bmatrix} \mathbf{v} \\
&= p(H_n) Q_n^\dagger \mathbf{v}
\end{aligned}$$

As a final step, notice that by construction the first row of $Q_n^\dagger$ is $\mathbf{v}/\|\mathbf{v}\|$, and all the remaining rows are orthogonal to $\mathbf{v}$, therefore only the first column of H_n, or the first n elements of the

first column of H are required to be 0. By Caylel-Hamilton theorem, this is guaranteed if we take $p = p^n$, where p^n is the characteristic polynomial of H_n. For the uniqueness part, suppose that there exists another polynomial, say q^n such that $q^n \perp \mathcal{K}_n$. But then $p^n - q^n$ is a nonzero polynomial of degree $n-1$ (because p^n, q^n are monic) such that $(p^n - q^n)(A)\mathbf{v} = \mathbf{0}$, and hence vectors $\mathbf{v}, A\mathbf{v}, \ldots, A^{n-1}\mathbf{v}$ are linearly dependent, which violates assumption that $\dim(\mathcal{K}_n) = n$.

■

This theorem allows us to interpret the Arnoldi eigenvalues estimates $\{\theta_i\}$ as the roots of the optimal polynomial. Following the above proof, it is relatively easy to see that they are scale-invariant, i.e. if $A \to \alpha A$ for some $\alpha \in \mathbb{C}$, then $\{\theta_i\}_{i=1}^n \to \{\alpha\theta_i\}_{i=1}^n$ and invariant under unitary transformations, i.e. if $A \to UAU^\dagger$ and $\mathbf{v} \to U\mathbf{v}$ for some unitary U, then the Arnoldi estimates are unchanged. Furthermore, owing to the properties of monic polynomials, they are also translationally invariant, namely if $A \to A + \alpha\mathbb{1}$ for some $\alpha \in \mathbb{C}$, then $\{\theta_i\}_{i=1}^n \to \{\theta_i + \alpha\}_{i=1}^n$.

In the end, we see that the direct purpose of Arnoldi iteration is to solve a polynomial approximation problem and not to find eigenvalues. However, those two problems have enough in common, that the Arnoldi iteration produces some correct eigenvalues as a 'by-product'. We can reason along the following lines. If our task is to find a polynomial $p \in P^n$ minimizing $\|p(A)\|$, it may be a good idea to select a polynomial that has roots close to the eigenvalues of A. In an extreme situation, when there exists a diagonalization of A and it posses only $n \ll m$ distinct eigenvalues, the minimal polynomial[2] will coincide with the characteristic polynomial computed via Arnoldi iteration after n steps and the Arnoldi eigenvalue approximations will be exact, provided we start from $\mathbf{v}$ having nonzero overlap with all eigenvectors of A. In most practical situations, however, the agreement is only approximate, namely Arnoldi eigenvalues are close to real eigenvalues, and computed polynomial is such that $\|p(A)\|$ is small.

There is more to this story than we have told here, particularly a nice geometric interpretation of Algorithm 1 via *Arnoldi lemniscates*, which illustrates why extremal eigenvalues are found first, however, we shall not concern ourselves with those matters any further. Interested readers are once again referred to Trefethen and Bau [61], whereas we turn our attention to the case of utmost interest in quantum mechanics, namely Arnoldi iteration for Hermitian matrices.

2.2.3 Restriction to Hermitian matrices: Lanczos iteration

After the mathematical detour of the previous section, armed with a deeper understanding of Krylov subspace and Arnoldi iteration, we are ready to investigate the algorithms that are of direct relevance to condensed matter physics, starting with Lanczos iteration. From this point onwards, we shall return to the favored by physicists Dirac bra-ket notation, namely $|v\rangle \equiv \mathbf{v}$ and $\langle v| = \mathbf{v}^\dagger$. Moreover, we assume the matrix A to be Hermitian, as in most use cases it will be the Hamiltonian of our system.

It immediately follows from (2.4) that, given A is Hermitian, the Hessenberg matrix H_n will also be Hermitian. But a matrix that is both Hessenberg and Hermitian, must of course

[2] A minimal polynomial of matrix A is a polynomial p of the smallest degree such that $p(A) = 0$. It always divides the characteristic polynomial.

be tridiagonal! Indeed, to see this directly, let us write the equation for matrix elements $(H_n)_{ij}$ of H_n:

$$(H_n)_{ij} = \sum_{r,s} (Q_n^\dagger)_{ir} (A)_{rs} (Q_n)_{sj} = \langle q_i | A | q_j \rangle \tag{2.6}$$

where $|q_i\rangle, |q_j\rangle$ are respectively i-th and j-th columns of matrix Q_n. From the recurrence relation (2.3) we know that $A|q_j\rangle \in \text{span}\{|q_1\rangle, \ldots, |q_{j+1}\rangle\}$, and that it is orthogonal to all $|q_i\rangle$ with $i > j+1$. Therefore $(H_n)_{ij} = 0$ for $i > j+1$. Similarly, by taking the Hermitian conjugate of equation (2.6), we get

$$(H_n)_{ij} = \langle q_j | A^\dagger | q_i \rangle \triangleq \langle q_j | A | q_i \rangle \tag{2.7}$$

where $\triangleq$ follows from assumed hermiticity of A. Repeating the above reasoning we quickly obtain that $(H_n)_{ij} = 0$ also for $j > i+1$ and hence the matrix is tridiagonal. In literature the diagonal is usually denoted by $\alpha_i \equiv (H_n)_{ii}$, whereas the sub- and superdiagonal are denoted by $\beta_i \equiv (H_n)_{i,i+1} = (H_n)_{i+1,i}$. The relation for $|q_{n+1}\rangle$ becomes a 3-step recurrence:

$$|q_{n+1}\rangle = \frac{A|q_n\rangle - \beta_{n-1}|q_{n-1}\rangle - \alpha_n |q_n\rangle}{\beta_n} \tag{2.8}$$

This has a tremendous impact on the practical applications of the algorithm, as both computational and memory costs decrease significantly. We are now ready to state the simplified version of the Algorithm 1. Another important observation is that α_n's are diagonal elements

Algorithm 2 Lanczos iteration

Input: $|v\rangle \in \mathbb{C}^m$, $A \in \mathbb{C}^{m\times m}$ such that $A^\dagger = A$, number of steps n

Output: columns of Q_n, tridiagonal matrix H_n

$\beta_0 = 0$
$|q_0\rangle = \mathbf{0} \in \mathbb{C}^m$
$|q_1\rangle = |v\rangle / \||v\rangle\|$
for $i = 1 : n-1$ **do**
    $|q\rangle = A|q_i\rangle$
    $\alpha_i = \langle q_i | q \rangle$
    $|q\rangle = |q\rangle - \beta_{i-1}|q_{i-1}\rangle - \alpha_i |q_i\rangle$
    $\beta_i = \||q\rangle\|$
    $|q_{i+1}\rangle = |q\rangle / \beta_i$
end for

of a Hermitian matrix, and β_n's are norms of the vector $|q\rangle$ in subsequent iterations, both of which are real. Therefore, even if our Hamiltonian is complex, the numbers α_n and β_n can be stored as vectors of real floating point numbers, decreasing memory requirements even further. Matrix Q_n is of dimension $m \times n$, so keeping it in full in the memory can still be costly. Fortunately, at each step of the Lanczos iteration, no more than three vectors are necessary ($|q\rangle, |q_i\rangle, |q_{i-1}\rangle$) so the storage of full matrix Q_n is reduntant. Extremal eigenvalues are then obtained by explicit diagonalization of the constructed matrix $H_n = V_n D_n (V_n)^\dagger$, which can be done efficiently using specialized routines for tridiagonal matrices. However, this approach has its drawbacks when we are interested also in the ground state eigenvector, which will be the case in further applications.

It turns out that the Lanczos iteration can approximate not only eigenvalues, but also corresponding eigenvectors. They are the eigenvectors of the tridiagonal matrix H_n, transformed back to the original Hilbert space. Given the full Hessenberg decomposition, we would have

$$A = QHQ^\dagger = Q(VDV^\dagger)Q^\dagger = (QV)D(QV)^\dagger \tag{2.9}$$

Restriction to n-step iteration produces an approximation $A \approx (Q_nV_n)D_n(Q_nV_n)^\dagger$. The simplest form of Lanczos iteration presented in Algorithm 2 is sufficient to obtain only the ground state eigenvector with machine precision because eigenvectors of excited states are plagued by the loss of orthogonality stemming from the nature of floating point numbers. We shall have a brief look at this problem at the end of this section.

The ground state vector $|\psi_0\rangle$ can be then read of as the first column Q_nV_n. However, there is a problem. To conserve memory, we have not constructred the whole matrix Q_n explicitly, but only three of its columns at a given time and hence do not have access to the matrix product Q_nV_n. We need a second pass of the Lanczos iteration, with a single line added for iterative calculation of the first column. It can be summarized by the the following piece of pseudocode:

Algorithm 3 Second pass of Lanczos iteration, for calculating ground state eigenvector

Input: $|\psi_0\rangle = \mathbf{0} \in \mathbb{C}^m$, matrix V_n from Alg. 2, rest of input data from Alg. 2

Output: columns of Q_n, tridiagonal matrix H_n

$\beta_0 = 0$
$|q_0\rangle = \mathbf{0} \in \mathbb{C}^m$
$|q_1\rangle = |v\rangle / \||v\rangle\|$
for $i = 1 : n-1$ **do**
    $|\psi_0\rangle = |\psi_0\rangle + (V_n)_{i,1} |q_i\rangle$ ▷ this is the only difference from Alg. 2
    $|q\rangle = A |q_i\rangle$
    $\alpha_i = \langle q_i|q\rangle$
    $|q\rangle = |q\rangle - \beta_{i-1} |q_{i-1}\rangle - \alpha_i |q_i\rangle$
    $\beta_i = \||q\rangle\|$
    $|q_{i+1}\rangle = |q\rangle / \beta_i$
end for

To finish this section, let us discuss quickly the convergence properties of Lanczos iteration. We have one free parameter, namely the number of iterations n. If we had carried out the full Arnoldi iteration, as described in 1, the orthogonality of subsequent columns of matrix Q_n would be guaranteed by the explicit Gram-Schmidt procedure and we in principle could continue it up to $n = m$ obtaining the full Hessenberg decomposition. However, restricting ourselves to a three-step recurrence in Lanczos iteration we rely on mathematical identities to force the orthogonality of $|q_i\rangle$ with all previous vectors. Those are valid in exact arithmetic, but can quickly break down when using floating point numbers, as it is done in practice. Therefore, the iteration is unstable and should be stopped as soon as the desired accuracy is reached. Taking E_n^1 to be the lowest eigenvalues of H_n, the convergence criterion can be defined as $|E_{n+1}^1 - E_n^1|/|E_n^1| < \varepsilon$ for some small ε, e.g. 10^{-14}. As long as it is nondegenerate, the convergence usually happens quite quickly for both the lowest eigenvalue and corresponding

eigenvector. To reliably obtain higher eigenstates one needs to perform reorthogonalization, but it requires keeping the matrix Q_n in memory which can be very costly.

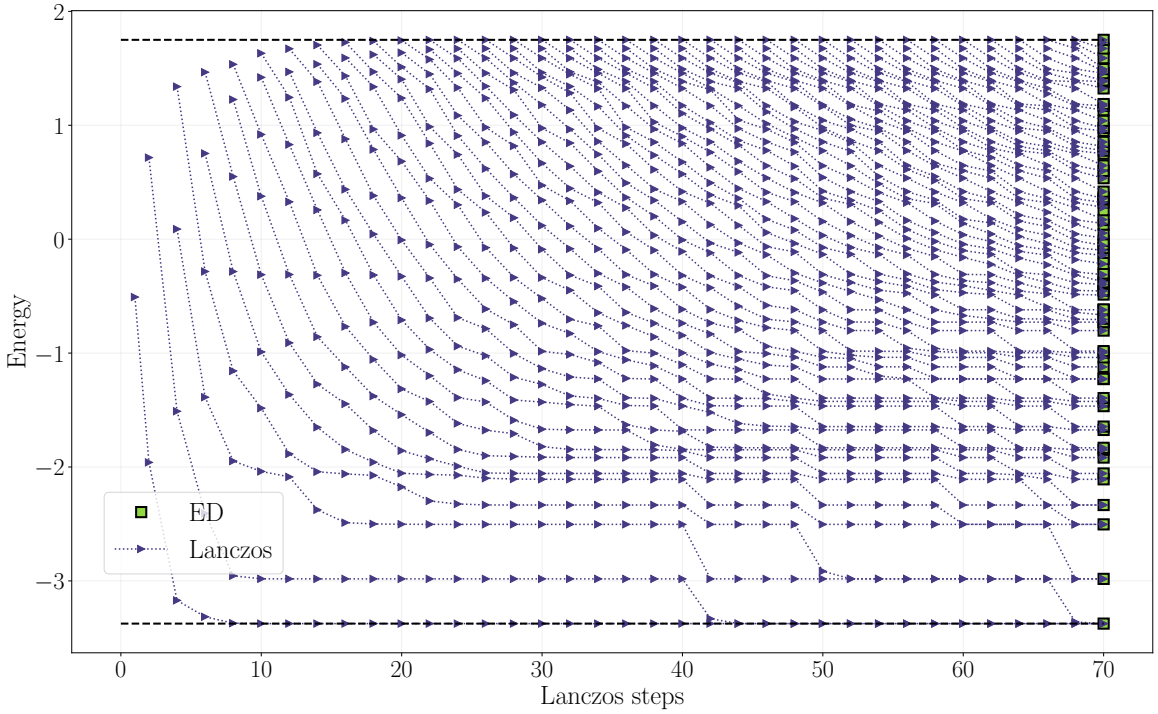

Figure 2.3: Plot of Arnoldi eigenvalues as a function of Lanczos steps, for a XXZ chain on 8 sites in the subspace with 0 total magnetization. The extremal eigenvalues converge very quickly to the values matching Exact Diagonalization. The numerical instability of Lanczos iteration is especially visible for a few lowest eigenvalues, where multiple ghosts start appearing. After $\binom{8}{4} = 70$ Lanczos steps, we should observe the exact spectrum emerging from Arnoldi approximates. However, we see that the ground state is triple degenerated, instead of unique as it should be.

This instability can manifest itself in an interesting way, namely in the form of additional eigenvalues, called Lanczos 'ghosts'. They are spurious copies of already found eigenvalues, which start apperating after too many iteration steps (cf. Fig. 2.3) They are difficult to understand rigorously, however Trefethen and Bau [61] offers a nice heuristic explanation. Reaching convergence of some Arnoldi approximated eigenvalue to the true eigenvalue of A causes annihilation of the corresponding eigenvector component in the vector $|q\rangle$. However, rounding errors originating from floating-point arithmetic cause $|q\rangle$ to again develop a component in the direction of the eigenvector and thus, after a certain number of iterations, the appearance of another Arnoldi approximated eigenvalue is necessary to annihilate it. This can go on and on producing more and more Lanczos 'ghosts'. Fortunately, for all further applications in this thesis, we will only require the lowest eigenstate, so we can avoid most of the instability problems by stopping the iteration sufficiently quickly.

2.3 Time evolution via the Krylov propagator

Even though the original purpose of Lanczos iteration was to approximate boundaries of the spectrum of matrices and solve systems of linear equation [106, 107], it can also be employed to evaluate functions of Hermitian matrices. Given any unitary (or orthogonal) decomposition of the matrix $A = QHQ^\dagger$, and an analytic function f[3], we have $f(A) = Qf(H)Q^\dagger$. And indeed, Lanczos iteration gives us such decomposition, albeit an approximate one $A \approx Q_n H_n Q_n^\dagger$. Because of this approximate character and convergence problems discussed at the end of the previous section, the global approximation of $f(A)$ via Lanczos iteration is a hopeless endeavor. However, the goal of this section is to calculate time evolution, which boils down to the evaluation of how the time-evolution operator $\exp\left(-i\hat{H}t\right)$ acts on some state $|v\rangle$ in the Hilbert space for a given Hamiltonian $\hat{H}$. It is thus enough to restrict our attention to the problem of calculating $f(A)|v\rangle$, for which the Lanczos iteration turns out to be an excellent tool.

Let us now assume that the matrix A is our Hamiltonian $\hat{H}$, acting on Hilbert space $\mathcal{H} \cong \mathbb{C}^m$ and $|v\rangle \in \mathcal{H}$ is some fixed state. Using the approximate factorization derived from (2.9), we get

$$f(\hat{H})\,|v\rangle \approx (Q_n V_n) f(D_n)(Q_n V_n)^\dagger\,|v\rangle \tag{2.10}$$

where D_n is a real diagonal matrix, so $f(D_n)$ is easy to compute. Previously, we have started the construction of the Krylov subspace basis from some random vector. Now, let us change this slighlty and start from the vector $|v\rangle$ instead, which we assume to be normalized. Then, the first column of Q_n will be $|v\rangle$, whereas all subsequent columns will be orthogonal (up to some numerical errors), yielding $Q_n^\dagger\,|v\rangle = |e_1\rangle$, which is the first vector in canonical basis of $\mathbb{C}^n$, i.e. $|e_1\rangle = [1, 0, 0, \ldots, 0]$. Equation (2.10) then simplifies to

$$f(\hat{H})\,|v\rangle \approx Q_n(V_n f(D) V_n^\dagger)Q_n^\dagger\,|v\rangle = Q_n(V_n f(D)V_n^\dagger)\,|e_1\rangle = Q_n f(H_n)\,|e_1\rangle \tag{2.11}$$

Moreover, $f(H_n)\,|e_1\rangle$ is just the first column of $f(H_n)$, because $(f(H_n)\,|e_1\rangle)_i = \sum_j (f(H_n))_{i,j}\,\delta_{1,j} = (f(H_n))_{i,1}$. So we do not need to compute the full matrix, but only a single vector of the form

$$(f(H_n))_{i,1} = \sum_j (V_n)_{i,j}\, f(D_n)_j \left(V_n^\dagger\right)_{j,1} = \sum_j (V_n)_{i,j}\,(V_n^*)_{1,j}\, f(D_n)_j \tag{2.12}$$

where the diagonal matrix $f(D_n)$ is treated as a vector. Assuming that $f(D_n)$ is already computed, it boils down to a single dot product for each element of the column.

We are now ready to apply this procedure to the problem of interest, namely the time-evolution of a pure state $|\psi(t)\rangle$ in the interval $(t, \Delta t)$. It is described by the Schrödineger equation $i\partial_t\,|\psi(t)\rangle = \hat{H}\,|\psi(t)\rangle$, having a formal solution

$$|\psi(t+\Delta t)\rangle = \exp\left(-i\hat{H}\Delta T\right)|\psi(t)\rangle\,, \tag{2.13}$$

under the assuption that $\hat{H}$ does not depend explicitly on time. The exact exponentiation of the matrix amounts to exact diagonalization which, as mentioned at the beginning of this

[3] A function f is real (complex) analytic if and only if its Taylor series about x_0 converges in some neighborhood of x_0 pointwise to the function, for every x_0 in the domain.

chapter, is a difficult task. However, by letting $f(\hat{H}) = \exp\left(-i\hat{H}\Delta t\right)$ and $|v\rangle = |\psi(t)\rangle$ in equation (2.11) we get an approximation of the action of the time evolution operator on a state, called the **Krylov based propagator** [108], which was originally proposed in the 1980's by Park and Light [63] and has been since used with great success to investigate many different systems [109–112]. The final equation reads

$$|\psi(t+\Delta t)\rangle = \exp\left(-i\hat{H}\Delta T\right)|\psi(t)\rangle \approx Q_n \exp\left(-iH_n\Delta t\right) Q_n^\dagger |\psi(t)\rangle \tag{2.14}$$

$$= Q_n \exp\left(-iH_n\Delta t\right)|e_1\rangle = \sum_{j=1}^{n} \left(f(H_n)\right)_{j,1} |q_j\rangle \tag{2.15}$$

where $|q_j\rangle$ are columns of the unitary (orthogonal) matrix Q_n. Because of this orthogonality, the approximation error is bounded from above by the last coefficient $\left(f(H_n)\right)_{n,1}$, i.e.

$$\left\| |\psi(t+\Delta t)\rangle_{\text{exact}} - |\psi(t+\Delta t)\rangle_{\text{Krylov}} \right\| \leq \left| \left(f(H_n)\right)_{n,1} \right| \tag{2.16}$$

assuming that $\||\psi(t)\rangle\| = 1$. There also exists an estimate of the sufficient dimension of Krylov subspace [113]

$$n \lessapprox 1.5\rho_{\hat{H}}\Delta t > 10 \tag{2.17}$$

where $\rho_{\hat{H}}$ is the spectral radius of Hamiltonian and can be calculated as the difference between the highest and lowest eigenvalue. It is now very simple to cast these expressions into a concrete algorithm

Algorithm 4 Krylov propagator

Input: input data from Algorithm 2, with $|v\rangle = |\psi(t)\rangle$, time step Δt

Output: propagated state $|\psi(t+\Delta t)\rangle$

1: Run Alg. 2, obtaining eigenvalues D_i
2: Calculate $\left(f(H_n)\right)_{i,1}$ using eq. (2.12)
3: Run modified Alg. 3, with $\left(f(H_n)\right)_{i,1}$ instead of $(V_n)_{i,1}$

We finish this section with a remark, that the real-time propagator is not the only function of the Hamiltonian which can be calculated using Lanczos techniques. Fairly often encounterd are also the imaginary-time propagator $\exp\left(-\beta H\right)$ and pure state Green's function of some obervable Q: $\langle\psi_{\epsilon_0}| Q \left(\omega + i\eta + \epsilon_0 + H\right)^{-1} Q |\psi_{\epsilon_0}\rangle$ [114]. However, we will not need them for this thesis.

2.4 Correlation functions and Quantum Typicality

We are now ready to introduce **time dependent correlation functions** and a method of calculating them using already developed Krylov subspace machinery. This function is defined for a pair of operators A, B as

$$\tilde{C}_{AB}(t) \equiv \mathrm{Re}\langle A(t)B\rangle = \mathrm{Re}\,\mathrm{Tr}\left(\hat{\rho}A(t)B\right) \tag{2.18}$$

where $\hat{\rho} = e^{-\beta H}/\mathcal{Z}$, $\mathcal{Z} = \mathrm{Tr}\left(e^{-\beta H}\right)$ is the canonical ensemble at temperature $T = 1/\beta$, and $A(t) = e^{i\hat{H}t}Ae^{-i\hat{H}t}$ is understood via the Heisenberg picture. In this thesis we are interested

only in the infinite temperature properties, so $\hat{\rho} \to \frac{1}{\mathcal{D}}\mathbb{1}$, where $\mathcal{D}$ is the dimension of Hilbert space, however, lets us keep the temperature finite for a while, so we can see the results of subsequent developments in full. Correlation functions allow us to probe the complex dynamics of interacting many-body systems and within Linear Response Theory are directly related to the transport properties [115], so they have been an object of intense study [116–122]. We can use a complete set of eigensetates $|n\rangle$ of the Hamiltonian $\hat{H}$ in order to transform the correlation function into the so-called spectral representation

$$\begin{aligned}
\langle A(t)B\rangle &= \frac{1}{\mathcal{Z}}\operatorname{Tr}\left(A(t)Be^{-\beta H}\right) = \frac{1}{\mathcal{Z}}\operatorname{Tr}\left(e^{i\hat{H}t}Ae^{-i\hat{H}t}Be^{-\beta H}\right) \\
&= \frac{1}{\mathcal{Z}}\sum_{k}\sum_{m,n}\langle k|\,|n\rangle\langle n|\,e^{i\hat{H}t}Ae^{-i\hat{H}t}\,|m\rangle\langle m|\,Be^{-\beta H}\,|k\rangle \\
&= \frac{1}{\mathcal{Z}}\sum_{k}\sum_{m,n}\delta_{k,n}e^{i(\varepsilon_n-\varepsilon_m)t}e^{-\beta\varepsilon_k}\,\langle n|A|m\rangle\,\langle m|B|k\rangle \\
&= \frac{1}{\mathcal{Z}}\sum_{m,n}e^{i(\varepsilon_n-\varepsilon_m)t}e^{-\beta\varepsilon_n}\,\langle m|A|n\rangle^*\,\langle m|B|n\rangle
\end{aligned} \tag{2.19}$$

which is useful for calculations using Exact Diagonalization. Unfortunately, we have already established that ED calculations suffer greatly from the exponential growth of the Hilbert space. We would like to have a more efficient method for calculating $C_{AB}(t)$, capable of accessing larger systems sizes, far beyond the reach of ED. The question is, how the Krylov subspace methods developed so far can help us? After all, we only know how to find the ground state and calculate the time evolution of any state, whereas calculating a correlation function requires taking the trace over a full ensemble of states. This is where the concept of **(Dynamical) Quantum Typicality** ((D)QT) comes into play, which broadly speaking postulates that a set of states with a common feature e.g. the same energy, should give a narrow distribution of some other feature e.g. expected value of some observable [123]. For pedagogical purposes, we shall now briefly review two approaches to (D)QT, first in Sec. 2.4.1 following the article by Popescu et al. [102] focusing on a conceptual point of view, and second in Sec. 2.4.2 following Bartsch and Gemmer [123] and Steinigeweg et al. [124], giving us a concrete numerical tool for evaluating correlation functions, complete with rigorous error analysis.

2.4.1 General Canonical Principle

Roughly speaking, Quantum Typicality is an attempt to replace the fundamental postulate of statistical mechanics [1], the equal *a priori* probability postulate, by a fundamentally different principle, referring not to statistical ensembles or time averages, but to individual states. Another key characteristic of this new postulate, dubbed **general canonical principle** [102] or **canonical typicality** [101] is the existence of a rigorous mathematical proof, unlike in the case of equal *a prior* probability postulate. Let us now consider an isolated quantum system, called the universe U, partitioned into two components, the system S and the much larger environment E. In the language of Hilbert spaces, this decomposition is $\mathcal{H}_U = \mathcal{H}_S \otimes \mathcal{H}_E$ such that $\mathcal{D}_s = \dim(\mathcal{H}_S) \ll d_E = \dim(\mathcal{H}_E)$. We can also impose some global constraint R for the universe, represented as restriction of the allowed states to some subspace $\mathcal{H}_R \subseteq \mathcal{H}_S \otimes \mathcal{H}_E$.

We take the restricted universe to be in a maximally entangled state

$$\rho_R = \frac{1}{\mathcal{D}_R}\mathbb{1}_R \tag{2.20}$$

capturing our lack of knowledge about the system and being consistent with our intuition from statistical mechanics, about assigning *a priori* equal probability to each pure state. Now, we define a canonical state of our system S, as the density matrix obtaiend from ρ_R by tracing out the degrees of freedom of the environment E

$$\rho_S^{\mathrm{C}} = \mathrm{Tr}_E\left(\rho_R\right) \tag{2.21}$$

The crucial insight of canonical typicality is that we can take the universe to be in some pure state $\rho_R = |\psi\rangle\langle\psi|$ and the state of the system

$$\rho_S(\psi) = \mathrm{Tr}_R\left(|\psi\rangle\langle\psi|\right) \tag{2.22}$$

will be very close to the canonical state ρ_S^{C}. Moreover, this 'closeness' can be quanitfied very precisely, using a mathematical result from the asymptotic theory of finite dimensional normed spaces called Levy's lemma [125], which tells us about the properties of typical points on high-dimensional hyperspheres. Because of normalization, pure quantum states can be represented as the point of a hypersphere, hence the lemma is applicable. Let us now introduce some concepts necessary for the precise statement of the result. A precise notion of distance between two objects requires a metric and in our case a suitable metric will be induced by a norm on the vector space of operators. There are two norms relevant for this problem, the **trace norm**

$$\|\rho\|_1 = \mathrm{Tr}\,|\rho| = \mathrm{Tr}\left(\sqrt{\rho^\dagger\rho}\right) \tag{2.23}$$

and the **Hilbert-Schmidt norm**

$$\|\rho\|_2 = \sqrt{\mathrm{Tr}\left(\rho^\dagger\rho\right)}\,. \tag{2.24}$$

The trace norm is used directly in the preciste statements of the general canonical principle, because $\|\rho_1 - \rho_2\|_1$ quantifies how hard is to tell apart ρ_1 and ρ_2 using measurements. Indeed, it can be shown that $\|\rho\|_1 = \sup_{\|A\|\leq 1}\mathrm{Tr}(\rho A)$, where $\|\cdot\|$ is the operator norm. The Hilbert-Schmidt norm is used during the proof, as it is a bit easier to manipulate and can be easily related to the trace norm using Jensen's inequality [126] for convex functions applied to $\phi(x) = x^2$. Taking $\{\lambda_i\}_{i=1}^{\mathcal{D}}$ to be the eigenvalues of ρ we have

$$\begin{aligned}\|\rho\|_1^2 &= \left(\sum_{i=1}^{\mathcal{D}}|\lambda_i|\right)^2 = \mathcal{D}^2\left(\sum_{i=1}^{\mathcal{D}}\frac{1}{\mathcal{D}}|\lambda_i|\right)^2 = \mathcal{D}^2\phi\left(\sum_{i=1}^{\mathcal{D}}\frac{1}{\mathcal{D}}|\lambda_i|\right)\\ &\leq \mathcal{D}^2\sum_{i=1}^{\mathcal{D}}\frac{1}{\mathcal{D}}\phi\left(\lambda_i\right) = \mathcal{D}\sum_{i=1}^{\mathcal{D}}|\lambda_i|^2 = \mathcal{D}\|\rho\|_2^2\end{aligned} \tag{2.25}$$

Hence, $\|\rho\|_1 \leq \sqrt{\mathcal{D}}\|\rho\|_2$. We shall meet the Hilbert-Schmidt norm again in the next section, when discussing the algorithm searching for local integrals of motion. The precise theorem establishing the typicality is as follows

Theorem 2.2 *Let V be a function assigning to each subset of $\mathcal{H}_U$ its volume (in the sense of a suitable Haar measure [125]). Then, the following inequality holds*

$$\frac{V\left[\{|\psi\rangle \in \mathcal{H}_R \mid \frac{1}{2}\|\rho_S(\psi) - \rho_S^{\mathrm{C}}\|_1 \geq \eta\}\right]}{V\left[\{|\psi\rangle \in \mathrm{H}_R\}\right]} \leq \eta' \tag{2.26}$$

where

$$\eta = \epsilon + \frac{1}{2}\sqrt{\frac{\mathcal{D}_S}{\mathcal{D}_E^{\mathrm{eff}}}}$$
$$\eta' = 4e^{-\frac{2}{9\pi^3}\mathcal{D}_R\epsilon^2}$$

and the effective dimension of environment subspace is $\mathcal{D}_E^{\mathrm{eff}} = \frac{1}{\mathrm{Tr}\left(\rho_E^2\right)} \geq \frac{\mathcal{D}_R}{\mathcal{D}_S}$, where $\rho_E = \mathrm{Tr}_S\left(\rho_R\right)$.

Mathematically inclined readers are referred to Popescu et al. [127] for the full proof of this theorem, but for us it is important what this theorem means, namely that all but exponentially rare pure states of the universe are on the level of the system indistinguishable from the canonical state ρ_S^{C}. For our purposes in this thesis, we are interested in the case where the constraint R is that the total energy in the universe is close to some fixed value E. Assuming that the system is weakly coupled with the environment, it becomes a standard exercise in statistical mechanics to show that the canonical state is the Gibbs canonical ensemble

$$\rho_S^{\mathrm{C}} \propto \exp\left(-\frac{H_S}{k_B T}\right) \tag{2.27}$$

where H_s is the Hamiltonian of the system and T is the temperature set by the energy E.

2.4.2 Dynamical Quantum Typicality

Another approach to Quantum Typicality is not concerned directly with quantum states, but with expectation values of quantum observables instead. It was shown that for states drawn from a particular distribution in Hilbert space, the expectation values of a generic observable Q are very similar [128]. This result was further extended in the case of a unitarly invariant probability distribution, that is normalized states of the form

$$|\psi\rangle = \sum_{i=1}^{\mathcal{D}} c_i |i\rangle \tag{2.28}$$

where $\mathrm{Re}\, c_i$ and $\mathrm{Im}\, c_i$ are drawn from multidimensional Gaussian distribuion with zero mean, and $\{|i\rangle\}_{i=1}^{\mathcal{D}}$ is an arbitrary basis. Technicaly, because $\sum_{i=1}^{\mathcal{D}} |c_i|^2 = 1$, the coefficients are not independent, thus the full distribution is not necessarily Gaussian. However, Central Limit Theorem ensures that for $\mathcal{D}$ suitably large the distribution is indeed close to Gaussian, with the standard deviation equal $1/\sqrt{2\mathcal{D}}$ [129]. Using the **Hilbert space average method**, analytical expressions for both the average HA and variance HV of $\langle\psi|Q|\psi\rangle$ were derived [123]. They are as follows

$$\mathrm{HA}\left[\langle\psi|Q|\psi\rangle\right] = \frac{\mathrm{Tr}\left(Q\right)}{\mathcal{D}} \tag{2.29}$$

$$\mathrm{HV}\left[\langle\psi|Q|\psi\rangle\right] = \frac{1}{\mathcal{D}+1}\left(\frac{\mathrm{Tr}\left(Q^2\right)}{\mathcal{D}} - \left(\frac{\mathrm{Tr}\left(Q\right)}{\mathcal{D}}\right)^2\right) \tag{2.30}$$

Proof of the above equations is not difficult conceptually, however, requires evaluation of rather cumbersome integrals over high-dimensional hyperspheres so we shall refrain from spelling it out in full. Interested readers can find all the details in a book by Gemmer et al. [129]. Let us now take $Q(t) = \hat{\rho}A(t)B$ and define a quantity

$$\alpha = \mathcal{D}\,\langle\psi|\sqrt{\hat{\rho}}A(t)B\sqrt{\hat{\rho}}|\psi\rangle \tag{2.31}$$

Note that because density matrix $\hat{\rho}$ is positive semi-definite and Hermitian, the square root $\sqrt{\hat{\rho}}$ exists and is well defined. The next step is to plug α into equations (2.29) and (2.30)

$$\mathrm{HA}\left[\alpha\right] = \mathrm{Tr}\left(\sqrt{\hat{\rho}}A(t)B\sqrt{\hat{\rho}}\right) = \mathrm{Tr}\left(\hat{\rho}A(t)B\right) = \frac{\mathrm{Tr}\left(e^{-\beta H}A(t)B\right)}{\mathcal{Z}} \tag{2.32}$$

$$\begin{aligned}\mathrm{HV}\left[\alpha\right] &= \frac{\mathcal{D}^2}{\mathcal{D}+1}\left(\frac{\mathrm{Tr}\left(\left(\sqrt{\hat{\rho}}A(t)B\sqrt{\hat{\rho}}\right)^2\right)}{\mathcal{D}} - \left(\frac{\mathrm{Tr}\left(\sqrt{\hat{\rho}}A(t)B\sqrt{\hat{\rho}}\right)}{\mathcal{D}}\right)^2\right) \\ &\leq \frac{\mathcal{D}}{\mathcal{D}+1}\,\mathrm{Tr}\left(\hat{\rho}A(t)B\hat{\rho}A(t)B\right) < \mathrm{Tr}\left(\hat{\rho}A(t)B\hat{\rho}A(t)B\right)\end{aligned} \tag{2.33}$$

Looking at eq. (2.32) we immediately see the desired way of calculating the correlation function.

$$\tilde{C}_{AB}(t) = \mathrm{Re}\,\frac{\mathrm{Tr}\left(e^{-\beta H}A(t)B\right)}{\mathcal{Z}} = \mathrm{Re}\,\frac{\mathcal{D}}{\mathcal{Z}}\,\langle\psi|e^{-\frac{\beta H}{2}}e^{iHt}Ae^{-iHt}Be^{\frac{-\beta H}{2}}|\psi\rangle + \mathrm{Re}\,\epsilon \tag{2.34}$$

where ϵ is the error we made by using just one random state $|\psi\rangle$. Let us massage this expression a bit more by introducing two auxiliary states $|\psi_\beta(t)\rangle = e^{-iHt}e^{-\frac{-\beta H}{2}}|\psi\rangle$ and $|\phi_\beta(t)\rangle = e^{-iHt}Be^{-\frac{-\beta H}{2}}|\psi\rangle$. We can also calculate the partition function using the random state $|\psi\rangle$ as

$$\mathcal{Z} = \mathrm{Tr}\left(e^{-\beta H}\right) = \mathcal{D}\,\langle\psi|e^{-\beta H}|\psi\rangle = \mathcal{D}\,\langle\psi_\beta(0)|\psi_\beta(0)\rangle \tag{2.35}$$

Combining (2.34) and (2.35), we arrive at the final expression, as seen in literature [116, 121, 122]

$$\tilde{C}_{AB}(t) = \mathrm{Re}\,\frac{\langle\psi_\beta(t)|A|\phi_\beta(t)\rangle}{\langle\psi_\beta(0)|\psi_\beta(0)\rangle} + \mathrm{Re}\,\epsilon \tag{2.36}$$

We have successfully shifted time evolution and the action of the density matrix to state vectors instead of operators, hence we may apply the Krylov time propagator, studied in the previous section, to calculate both real and imaginary time evolution. Apart from that, the only other numerical calculations are sparse matrix-vector multiplication[4] and inner products of vectors, which are much less demanding than full exact diagonalization.

The final thing left is to estimate the error ϵ, in order to show that this approach makes sense. From eq. (2.33) it is clear that the Hilbert Space Average of ϵ is zero, as

$$\mathrm{HA}(\epsilon) = \mathrm{HA}\left(\alpha - \mathrm{Tr}\left(\hat{\rho}A(t)B\right)\right) = 0 \tag{2.37}$$

[4]Matrices representing local observables will also be sparse.

Equation (2.33), for Hilber Space Variance, allows us to estimate the standard deviation

$$\begin{aligned}(\sigma(\epsilon))^2 &= \mathrm{HV}\left[\epsilon\right] = \mathrm{HV}\left[\alpha\right] < \mathrm{Tr}\left(\hat{\rho}A(t)B\hat{\rho}A(t)B\right) \\ &= \sum_{m,n} \frac{e^{-\beta\varepsilon_m}}{\mathcal{Z}} \langle m|A(t)B|n\rangle \frac{e^{-\beta\varepsilon_n}}{\mathcal{Z}} \langle n|A(t)B|m\rangle \\ &< \sum_{m,n} \frac{e^{-\beta\varepsilon_m}}{\mathcal{Z}} \langle m|A(t)B|n\rangle \frac{e^{-\beta\varepsilon_0}}{\mathcal{Z}} \langle n|A(t)B|m\rangle \\ &= \frac{1}{\mathrm{Tr}\left(e^{-\beta(H-\varepsilon_0)}\right)} \sum_{m} \frac{e^{-\beta\varepsilon_m}}{\mathcal{Z}} \langle m|A(t)BA(t)B|m\rangle \\ &= \frac{1}{\mathrm{Tr}\left(e^{-\beta(H-\varepsilon_0)}\right)} \mathrm{Tr}\left(\hat{\rho}A(t)BA(t)B\right) \end{aligned} \tag{2.38}$$

Where the red inequality follows from the fact that the Boltzmann factor is a strictly decreasing function and assuming that the spectrum of H is ordered in increasing fashion. Defining the effective dimension $\mathcal{D}_{\mathrm{eff}} \equiv \mathrm{Tr}\left(e^{-\beta(H-\varepsilon_0)}\right)$, we finally obtain the upper bound on a standard deviation of error as

$$\sigma\left(\mathrm{Re}\,\epsilon\right) < \sqrt{\frac{\mathrm{Re}\langle A(t)BA(t)B\rangle}{\mathcal{D}_{\mathrm{eff}}}} \tag{2.39}$$

From this bound, we see that at infinite temperature, the error is exponentially suppressed in system size, and thus for suitably large systems even a single pure state $|\psi\rangle$ is enough to obtain a very good approximation of the correlation function. It becomes progressively worse with lower temperature, however as the mean error is 0 we can always average over a few random states. Fortunately, in this thesis, we are only interested in case $\beta \to 0$, so usually a single run will be enough.

As an example application, in figure 2.4 we present the infinite-temperature spin current autocorrelation functions in the nearest-neighbor Heisenberg model, obtained by setting $r_{\mathrm{max}} = 1$ in equations (1.2) and (1.13).

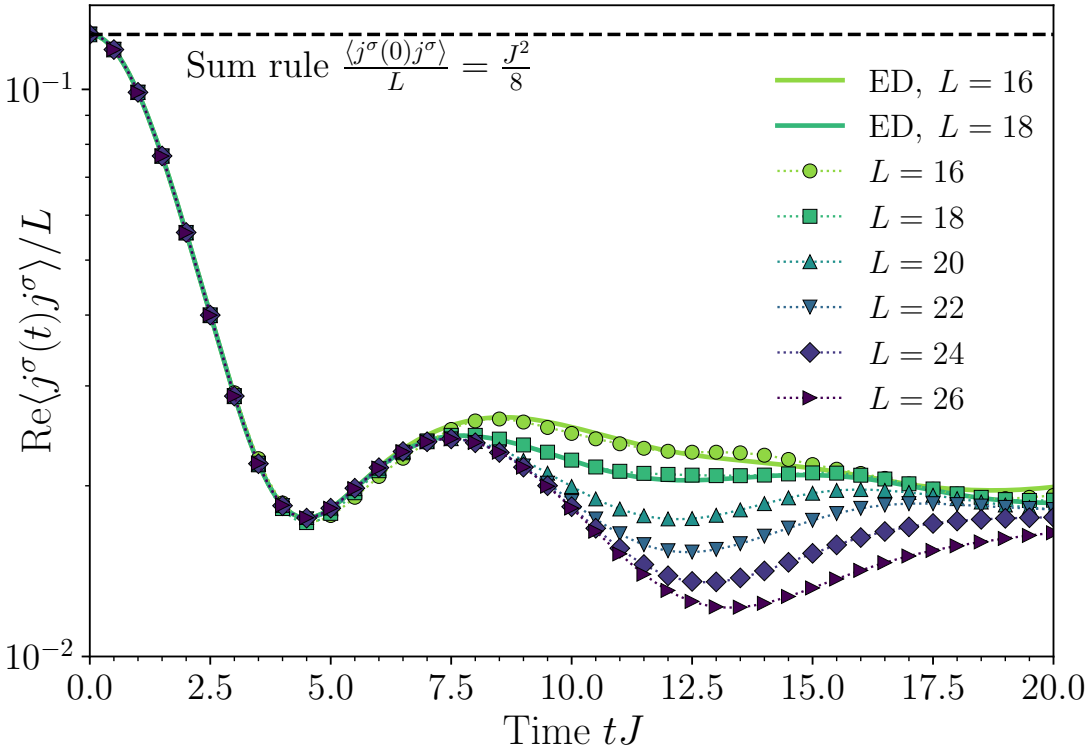

Figure 2.4: Infinite-temperature autocorrelation function of spin current j_σ in isotropic Heisenberg model ($J = 1,\ \Delta = 1$), evaluated using Exact Diagonalization for $L = 16,\ 18$ and Dynamical Quantum Typicality with Krylov propagator for $L = 16,\ 18,\ 20,\ 22,\ 24,\ 26$. Already for a modest size of $L = 18$ lattice sites we observe a very good agreement between ED and DQT calculation for a single pure state. Because of eq. (2.39), we expect this agreement to be exponentially better for larger system sizes.

3

Spin transport in long-range anisotropic Heisenberg model

After all the technicalities of the previous chapter, we are finally ready to study spin transport in the long-range anisotropic Heisenberg model. The main motivation of this investigation is the fact that this model admits two limits exhibiting ballistic spin transport (cf. Fig. 3.1), namely the free particles with nearest-neighbor hopping for $\alpha \to \infty$, $\Delta = 0$ and the Haldane-Shastry model with $J_{\mathrm{HS}(r)} = J \sin^2(\pi/L) / \sin^2(\pi r/L)$ for $\alpha = 2$ [130, 131]. In the latter case, this limit is only strictly valid in the thermodynamic limit, since $\sin^{-2}(r/L) \propto r^{-2}$ for $r \ll L$. In both of these limiting models the spin current j^σ commutes with the Hamiltonian and thus is strictly conserved. Hence, even though the Hamiltonian (1.2) is not integrable for arbitrary α, one could suspect that it will be *nearly integrable*, in the sense described in the introduction, and support interesting transport properties. Using spin density expansion and linear response theory of optical conductivity, in this chapter we will show that this is indeed the case and the spin transport is *quasibalistic* along a sharp line in the parameter space $\Delta \simeq \exp(-\alpha + 2)$, which continuously connects the two limiting cases mentioned above.

Results described in this chapter were first presented in chapters II and III of Mierzejewski et al. [96].

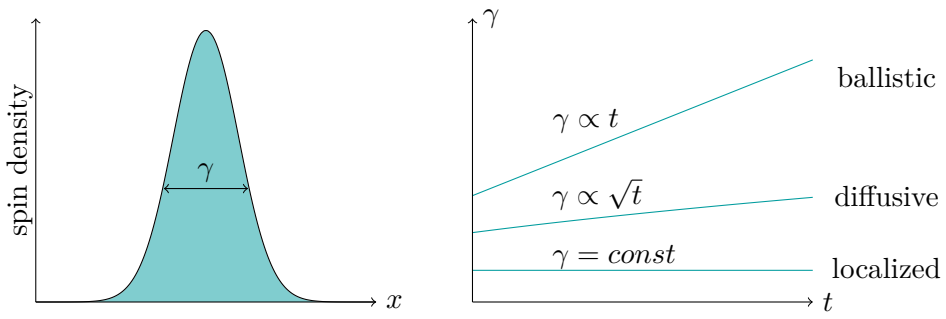

Figure 3.1: Illustration of different types of transport. On the left panel, we have some initial spin density characterized by width γ. On the right panel, we have the dependence of γ on time in three different cases.

3.1 Spin density expansion

Taking inspiration from experimental studies of cold atoms [92–94, 132], we consider an initial state in the form of a spin domain wall

$$|\psi(0)\rangle = |\underbrace{\uparrow\uparrow\uparrow\uparrow\uparrow}_{x}\underbrace{\downarrow\downarrow\downarrow\ldots\downarrow}_{L-x}\rangle\,,\ x = 5 \tag{3.1}$$

and study the dynamics of spin expansion by measuring the time dependence of the magnetization profile $M_\ell(t) = \langle\psi(t)|S^z_\ell|\psi(t)\rangle$. Such a product state initial configuration is desirable for two reasons. First, it is relatively accessible in experiments, e.g. using higher-order optical Stark shifts to rotate individual spins [133]. Second, from the theoretical point of view, by assuming open boundary conditions and choosing $x = 5$, we localize the domain wall close to the edge of the system, which allows us to avoid finite-size effects for longer times. Moreover, the dynamics generated by the Hamiltonian (1.2) conserve the total magnetization and hence we can restrict ourselves to the subspace of states with just 5 spins up. This considerably reduces the dimensionality of the problem and allows us to study systems as large as $L = 45$ with $\binom{45}{5} \approx 1.2 \times 10^6$ states, characterized by the total magnetization $M_{\text{tot}} = -35/2$. To put this into perspective, the full Hilbert space of such system has dimension 2^{45} which is $O(10^7)$ larger and thus completely inaccessible without additional techniques.

For the time evolution, we use the Krylov propagator introduced in detail in the previous chapter. A sample magnetization profile obtained for $\alpha = 3.5$ and $\Delta = 1.0$ is shown in Fig. 3.2. In order to quantitatively investigate the spin transport in this setup, we introduce

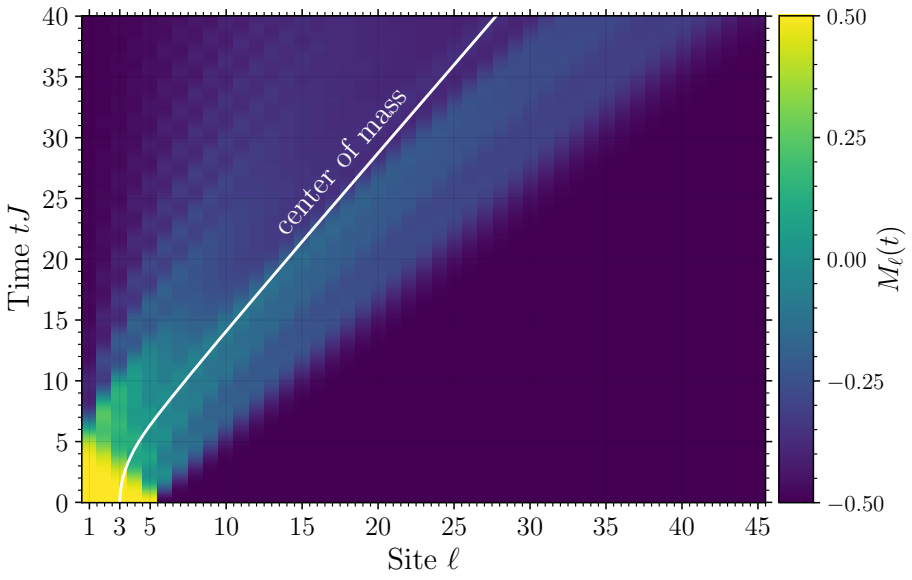

Figure 3.2: Time dependence of magnetization profile $M_\ell(t)$ for $\alpha = 3.5$ and $\Delta = 1.0$. The evolution of the center of mass, initially at $r_{\text{cm}}(t = 0) = 3$, is marked by a white line.

the so-called **center of mass**, defined as the first density moment of the magnetization profile

$$r_{\text{cm}}(t) = \frac{\sum_{\ell=1}^{L} \ell\,(M_\ell(t) + 1/2)}{\sum_{\ell=1}^{L} (M_\ell(t) + 1/2)} = \frac{\sum_{\ell=1}^{L} \ell\,(M_\ell(t) + 1/2)}{M_{\text{tot}} + L/2} \tag{3.2}$$

In Fig. 3.2, an example of time evolution of center of mass is shown. Examining $r_{\mathrm{cm}}(t)$ calculated for two values of $\Delta = 0.2,\ 0.5$ and various values of $\alpha \in \{2.0, 2.5, \ldots, 5.0\}$ (cf. Fig. 3.3), we observe a first hint of non-trivial transport properties of the model, namely non-monotonic dependence of $r_{\mathrm{cm}}(t)$ on α.

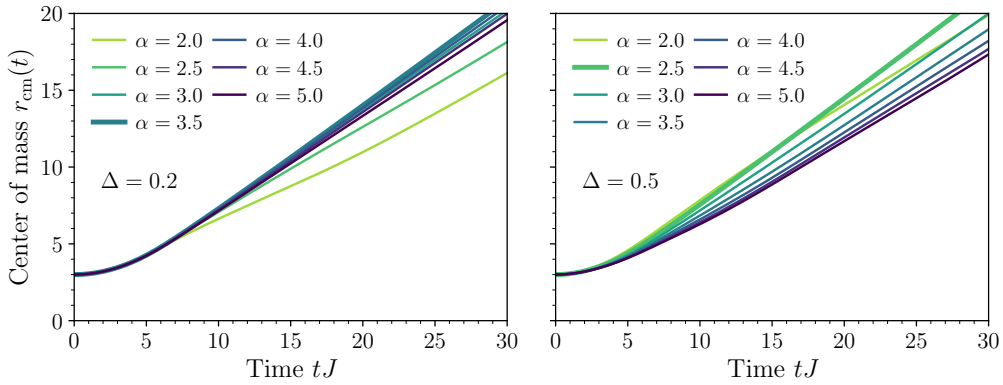

Figure 3.3: Time dependence of the center of mass $r_{\mathrm{cm}}(t)$ for $\Delta = 0.2$ (left panel) and $\Delta = 0.5$ (right panel) and various values of interaction decay α. The line corresponding to the fastest-moving center of mass is thicker than the rest.

To see this better, in Fig. 3.4 we look at the velocity obtained from the time derivative of the center of mass

$$\nu_{\mathrm{cm}}(t) = \frac{\mathrm{d}r_{\mathrm{cm}}(t)}{\mathrm{d}t}. \tag{3.3}$$

We observe that for both values of Δ, there is a clear maximum of the velocity of the expansion

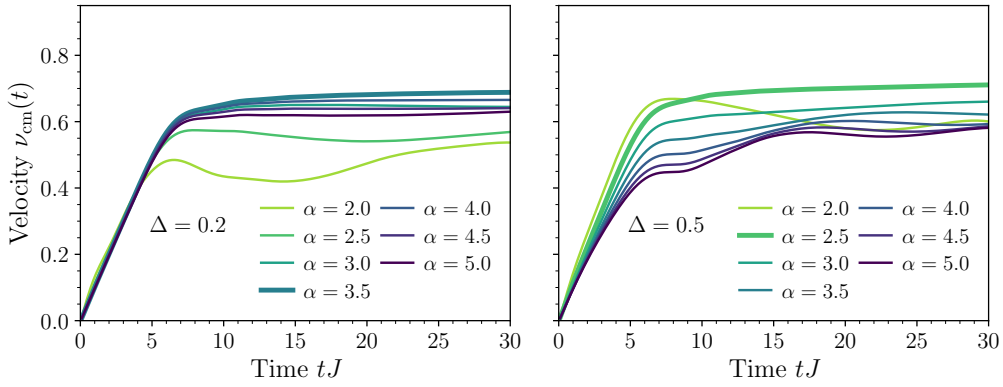

Figure 3.4: Time dependence of the velocity $\nu_{\mathrm{cm}}(t)$ for $\Delta = 0.2$ (left panel) and $\Delta = 0.5$ (right panel) and various values of interaction decay α. The line corresponding to the largest velocity is again thicker than the rest.

at some intermediate value of α. Investigating further the dependence of velocity on the parameters of the model, we calculate the average velocity $\bar{\nu}_{\mathrm{cm}}$ on the interval $t \in [20, 30]$ and plot it as a function of α for various values of Δ (cf. left panel of Fig. 3.5). The non-monotonic behavior is now evident, as for a fixed Δ, there exists a value of $\alpha = \alpha_{\nu_{\max}}(\Delta)$, such that the

average velocity has a maximum (for $\Delta = 0.0$ the optimal α is shifted to infinity). Equivalently, for each α there exists an optimal value of $\Delta = \Delta_{\nu_{\max}}(\alpha)$.

In the right panel of Fig. 3.5 we look at the dependence of average velocity on both parameters of the model. Moreover, we superimpose the points corresponding to the optimal anisotropies $\Delta_{\nu_{\max}}(\alpha)$. Curiously, these points seem to lie very close to an exponential curve, given by $\Delta_O = \exp(-\alpha + 2)$. Furthermore, as seen in the left panel, the average velocity is approximately constant for $\alpha \geq 2$ and equal to $\bar{\nu} \simeq J/\sqrt{2}$ along this line. Such velocity is a characteristic of ballistic transport in the nearest neighbors free-fermion model [93, 134], corresponding via Jordan-Wigner transformation to our model with $\alpha \to \infty$ and $\Delta = 0$. Therefore, we suspect that the optimal line $\Delta_{\nu_{\max}}(\alpha)$, present in this interacting system and indicating **quasibalistic** transport, is a transient remnant of the transport properties of the free fermions.

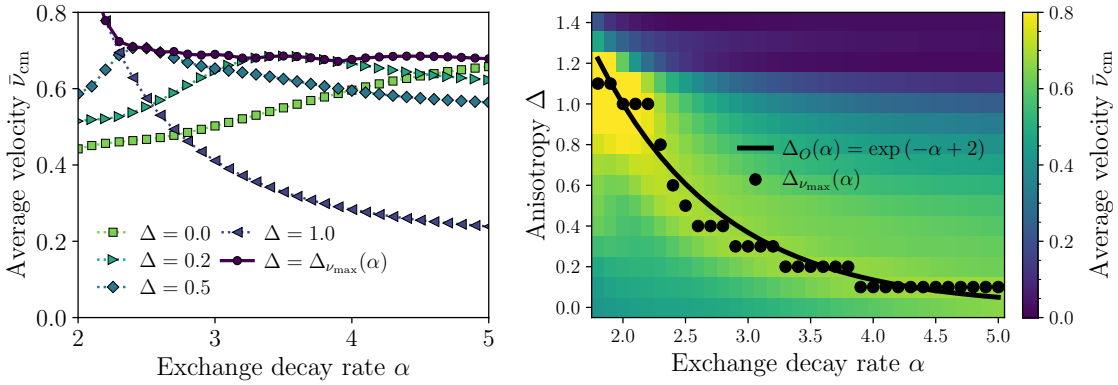

Figure 3.5: Left panel: average velocity $\bar{\nu}_{\rm cm}$ as a function of α for various values of Δ. Right panel: heatmap of the average velocity $\bar{\nu}_{\rm cm}$ as a function of α and Δ. The points corresponding to the optimal anisotropies $\Delta_{\nu_{\max}}(\alpha)$ are marked with black dots, while the solid line indicates the optimal line $\Delta = \Delta_O = \exp(-\alpha + 2)$.

3.2 Optical conductivity

In this section, we approach the problem of spin transport in the long-range Heisenberg model from the perspective of **linear response theory**. We study the **optical conductivity** [1] $\sigma(\omega)$ of the model, which is a measure of the response of the system to an external electromagnetic field. In the linear response regime, the optical conductivity is given by the Kubo formula, which for infinite temperature reads

$$\sigma(\omega) = \frac{\pi}{L\mathcal{Z}} \sum_{n,m} |\langle n|j^\sigma|m\rangle|^2 \delta(\omega - \epsilon_m + \epsilon_n) \tag{3.4}$$

where $\mathcal{Z}$ is the number of states in the Hilbert space, L is the system size and j^σ is the spin current operator (1.13), derived in Chapter 1. For the derivation of the Kubo formula and

[1] The optical conductivity is also known as the spin conductivity.

the optical conductivity, see Appendix B. As the sum in Eq. (3.4) runs uniformly over all many-body eigenstates $H|n\rangle = \epsilon_n|n\rangle$ of the Hamiltonian, this quantity probes the whole eigenspectrum. Equation 3.4 suggests a simple numerical procedure for calculating the optical conductivity. First, one needs to diagonalize the Hamiltonian H and obtain the eigenstates $|n\rangle$ and eigenvalues ϵ_n. Then, one needs to calculate the matrix elements of the spin current operator $\langle n|j^\sigma|n\rangle$ between all pairs of eigenstates. Finally, the optical conductivity is obtained by summing over all pairs of eigenstates, weighted by the corresponding matrix elements and the δ function. It is only the last step that requires some care, as the δ function is not a regular function and would require some binning of the discrete spectrum. We avoid this, by instead considering the **integrated conductivity**

$$\mathcal{I}(\Omega) = \frac{1}{\mathcal{S}_{\text{tot}}}\int_{-\Omega}^{\Omega} \mathrm{d}\omega\, \sigma(\omega) = \frac{\pi}{L\mathcal{Z}\mathcal{S}_{\text{tot}}}\sum_{n,m} |\langle n|j^\sigma|m\rangle|^2 \theta(\Omega - |\epsilon_m - \epsilon_n|) \tag{3.5}$$

where $\theta(x)$ is the Heaviside step function and $\mathcal{S}_{\text{tot}}$ is the sum rule

$$\mathcal{S}_{\text{tot}} = \int_{-\infty}^{\infty} \mathrm{d}\omega\, \sigma(\omega) = \frac{\pi}{L\mathcal{Z}}\sum_{n,m} |\langle n|j^\sigma|m\rangle|^2 \tag{3.6}$$

It is easy to see that the integrated conductivity $\mathcal{I}(\Omega)$ is a regular function of Ω, and contains the information about the fraction of the spectral weight contained in the frequency window $[-\Omega, \Omega]$. Equation (3.5) is now straightforward to evaluate numerically.

We evaluate the integrated conductivity (3.5) for the long-range Heisenberg model with periodic boundary conditions, and system sizes up to $L = 20$. We also restrict the calculations to the subspace of zero total magnetization, i.e. the largest sector with $\binom{L}{L/2}$ states. Leveraging the periodic boundary conditions, we perform the calculations separately for each momentum sector and then add the results together.

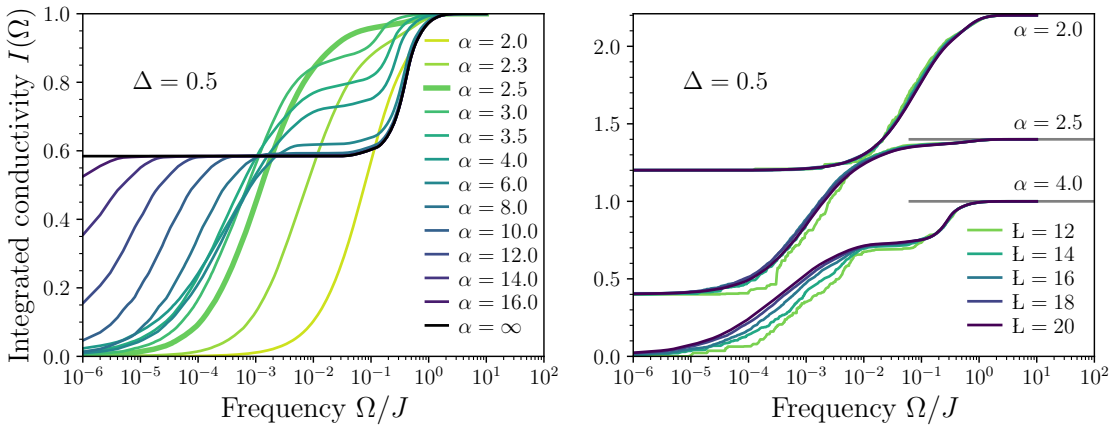

Figure 3.6: Left panel: Integrated conductivity $\mathcal{I}(\Omega)$ as a function of frequency window Ω for various values of α and $\Delta = 0.5$. The thicker line denotes the result for optimal decay parameter α. Right panel: Size dependence of the integrated conductivity $I(\Omega)$ for $\alpha = 2.0,\ 2.5,\ 4.0$ and $\Delta = 0.5$, illustrating the effects of finite size. For clarity, we added a vertical shift to distinguish the curves for different decay parameters.

Looking at the left panel of Fig. 3.6, we observe that the integrated conductivity for $\alpha \to \infty$ is exhibiting a **Drude peak** behavior at $\Omega \to 0$, and a distinct incoherent (regular) spectrum for $0.1 \lesssim \Omega/J \lesssim 1.0$, which is consistent with the results for the nearest neighbor Heisenberg model [135]. As α is decreased (the range of the interactions increases), but remains $\alpha \gtrsim 10$, the Drude peak becomes suppressed, while the regular part of the spectrum is still more or less the same. However, an interesting feature appears in the spectrum for $\alpha \lesssim 10$, namely the incoherent part starts shifting towards lower frequencies. For anisotropy $\Delta = 0.5$, this behavior is most pronounced for $\alpha = 2.5$, where the integrated conductivity is $\mathcal{I}(\Omega) \simeq 1$ for all $\Omega/J < 0.01$, which means that most of the spectral weight is contained in the frequency window $[-0.01, 0.01]$. This in turn implies ballistic-like spin transport for extremely long times up to $tJ \simeq 100$, similar to the case of noninteracting particles, as there we have $\sigma(\omega) \propto \delta(\omega) \implies I(\Omega) = 1$ for $\Omega > 0$. Furthermore, we once again observe some kind of non-monotonic behavior, as decreasing the decay parameter beyond $\alpha \approx 2.5$ shifts the incoherent part of the spectrum back towards higher frequencies.

To quantitatively investigate this effect across the parameter space, in Fig. 3.7 we present heatmaps of the integrated conductivity $\mathcal{I}(\Omega)$ on the (α, Ω) plane, for different values of the anisotropy Δ. Moreover, with a solid black line we denote the the value $\Omega = \Omega^*$, for which the integrated conductivity is $\mathcal{I}(\Omega^*) = 0.9$, i.e. 90% of the sum rule S_{tot}.

As in the case of average velocity during a spin expansion experiment, for every value of Δ, we can find a value of α for which the quantity telling about transiency of ballistic transport admits extremal value. Here, it is the Ω^* that becomes minimal, and in fact surprisingly small, implying transient ballistic spin transport. Once again, we can proceed in reverse, and extract the optimal anisotropy $\Delta_\sigma = \Delta_\sigma(\alpha)$ as a function of the decay parameter α, for which Ω^* is minimal. We can thus directly compare the optimal anisotropies obtained from the two different quantities, namely the average velocity and the integrated conductivity.

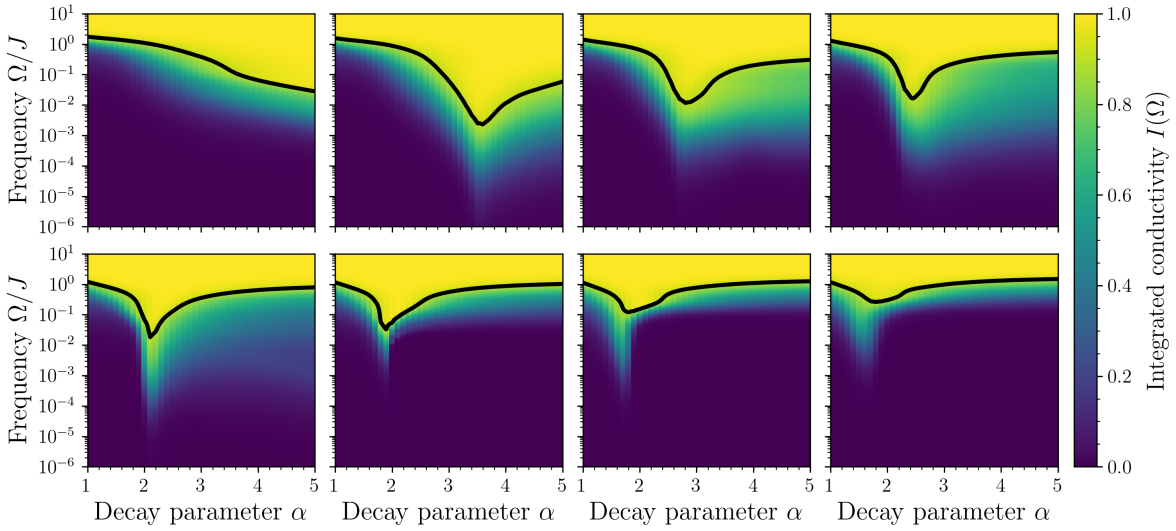

Figure 3.7: Heatmaps of the integrated conductivity $\mathcal{I}(\Omega)$ on the (α, Ω) plane. Black solid line denotes the value $\Omega = \Omega^*$, for which the integrated conductivity is $I(\Omega^*) = 0.9$.

The results are presented in Fig. 3.8, and we observe an excellent agreement between Δ_σ obtained from linear response theory, that is low frequency (long time) dynamics, of a system

with periodic boundary conditions, and the optimal anisotropy $\Delta_O(\alpha)$, inferred from the short-time spin domain expansion in a chain with open boundary conditions. This is a strong indication that the transient ballistic spin transport is a generic feature of the long-range Heisenberg model, and not an artifact of the finite system size. It is further supported by the finite-size analysis of the integrated conductivity, presented in the right panel of Fig. 3.6, where we observe that $\mathcal{I}(\Omega)$ for $\alpha = 2.0$ is almost independent of the system size, and for larger values of α, the incoherent part of the spectrum is shifted towards even lower frequencies.

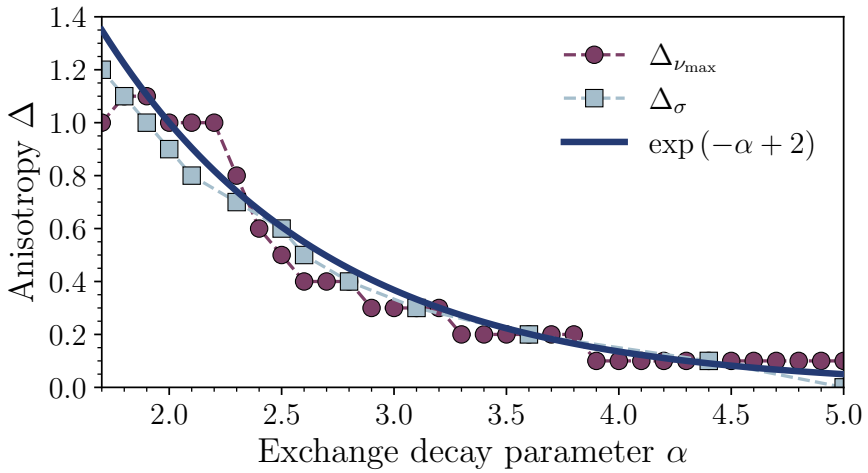

Figure 3.8: Optimal values of anisotropy Δ, as a function of decay parameter α, obtained from the average velocity of spin expansion and integrated conductivity. The solid line denotes the optimal line $\Delta_O = \exp(-\alpha + 2)$.

It is worth mentioning, that in Mierzejewski et al. [96], we have also looked into a generalized version of the aforementioned Haldane-Shastry model, with the exchange interaction of the form $J_{\mathrm{HS}(\alpha)} \propto 1/\sin^{\alpha}(\pi r/L)$. We have shown that it exhibits very similar behavior, with the integrated conductivity close to the one obtained for the long-range Heisenberg model, and the optimal anisotropy following the same exponential curve. Moreover, we have investigated two other models, namely the next-nearest neighbor Heisenberg model (i.e. (1.2) with $r_{\max} = 2$), and the long-range t-V spinless fermion model. Contrary to the nearest-neighbor case, the long-range t-V model is not related to the long-range Heisenberg model via the Jordan-Wigner transformation, and thus the two models are not equivalent. The former case yielded results similar to the long-range Heisenberg model for small values of anisotropy $\Delta \in [0, 0.2]$, while for larger values of Δ, the integrated conductivity was rather featureless. It is consistent with our main results, as is this parameter regime, the optimal decay is $\alpha \gtrsim 3.5$, rendering the terms with $r > 2$ insignificant. In the latter case of spinless fermions, the quasibalistic transport was all but absent. Therefore, it is expected that this phenomenon is unique to the long-range Heisenberg model. For more details about those results, that go beyond the scope of this thesis, the interested reader is referred to the original research article.

4

Slowly decaying eigenmodes

In the previous chapter, we have numerically shown the existence of optimal anisotropy $\Delta_O = \exp(-\alpha + 2)$, which ensures slow relaxation of the spin current j^σ (1.13) and consequently quasiballistic spin transport. Here, we will demonstrate that this feature is not unique to the spin current, but exhibited also by a class of other, *local* operators. To this end, we will employ an algorithm devised by Mierzejewski et al. [95], originally designed to identify local integrals of motion in integrable tight-binding models. As the model we are considering in this work is not integrable, we are not expecting to find strictly conserved quantities, but only so-called **local slowly relaxing operators (LSROs)**. We will interpret the discovered observables in terms of fermionic currents, describing particle hopping with various ranges. Moreover, we will also show how to improve the numerical efficiency of the algorithm, by utilizing symmetry subspaces and the Dynamical Quantum Typicality approach to correlation functions[1] (cf. section 2.4.2).

4.1 Detecting local slowly relaxing operators

4.1.1 Theoretical description

Let us start by introducing in detail the original algorithm for detecting local integrals of motion (LIOMs), following the original article by [95]. In principle, finding a **complete set of LIOMs** is a conceptually nontrivial task, however, this procedure reduces it to a simple application of linear algebra [95]. In this section, unless stated otherwise, by H we will denote an arbitrary tight-binding Hamiltonian with periodic boundary conditions on L sites, having eigenstates $H|n\rangle = \epsilon_n |n\rangle$. Moreover, for any operator A we define $A_{mn} \equiv \langle m|A|n\rangle$.

In order to employ techniques from linear algebra, we need to have a linear space of some kind. This role is played by the space of *local, traceless, and translationally invariant* observables, supported on up to M sites and acting on vectors from a Hilbert space $\mathcal{H}$ of dimension $\mathcal{D}$. We will denote this space by $\mathcal{V}_M$. Its building blocks are the spaces $\mathcal{V}^m$, of operators supported on exactly m sites, i.e. of the form

[1] And why it, unfortunately, fails in this case.

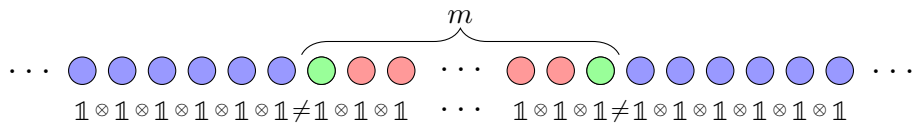

where blue circles correspond to single-site identity operators, green circles to an arbitrary single-site operator except for the identity and red circles to an arbitrary single-site operator. If we were to allow identity operators on green sites, we would have obtained a $(m-1)$-local operator. It is easy to see that an arbitrary linear combination of operators from $\mathcal{V}^m$ is again an element of $\mathcal{V}^m$, hence $\mathcal{V}^m$ is a linear space. Therefore, the full space

$$\mathcal{V}_M = \bigoplus_{m=1}^{M} \mathcal{V}^m \tag{4.1}$$

is also a linear space. We will always assume that $0 \leq M \leq L/2$.

Using the infinite temperature correlation function (cf. Eq. (2.18)) we can endow this space with an inner product

$$\mathcal{V}_M \times \mathcal{V}_M \ni (A,B) \mapsto (A|B) \equiv \frac{1}{\mathcal{D}} \operatorname{Tr}\left(AB^\dagger\right) = \frac{1}{D} \sum_{n,m=1}^{D} A_{nm} B^*_{nm} \in \mathbb{C} \tag{4.2}$$

called the **Hilbert-Schmidt inner product** and inducing the **Hilbert-Schmidt norm** $\|A\| = \sqrt{(A|A)}$. It is worth noting, that if we let the first operator be time-dependent, and consider the Hilbert-Schmidt inner product as a function of time, we obtain the infinite temperature correlation function (2.18). Because we only consider finite systems in this thesis, we do not need to worry about situations where the trace is not well defined. The pair $(\mathcal{V}_M, (\cdot|\cdot))$ is then a finite-dimensional Hilbert space. We are now able to state more precisely what we mean by a complete set of LIOMs. It is a set of local observables $\{Q_\beta : [Q_\beta, H] = 0\}$, such that for any observable A we have

$$\lim_{t\to\infty} (A(t)|A) = \sum_\beta \frac{(Q_\beta|A)^2}{(Q_\beta|Q_\beta)} \tag{4.3}$$

i.e. the completeness is understood as the saturation of the Mazur bound [136].

The mathematical stage is now set, so let us proceed further toward the algorithm. As $\mathcal{V}_M$ is a linear space, it possesses a basis $\{O_\gamma\}$, which with the help of the inner product can be made into an orthonormal basis $(O_\gamma|O_{\gamma'}) = \delta_{\gamma\gamma'}$. We can also think of this space as an orthogonal subspace of the space $\mathcal{V}$ of all possible operators acting on $\mathcal{H}$, in the sense that

$$(\forall A \in \mathcal{V})\,(A = A^M + A^\perp = \sum_\gamma (O_\gamma|A)\, O_\gamma + A^\perp),\ \text{such that}\ (\forall\gamma)\,((O_\gamma|A^\perp) = 0) \tag{4.4}$$

We will describe an example of such a basis in the next section, but for now, it is enough that it exists.

Next, we would like to determine the conserved part of all the basis operators O_γ. We do

this by considering the infinite time average

$$\begin{aligned}\bar{O}_\gamma = \lim_{\tau\to\infty}\frac{1}{\tau}\int_0^\tau \mathrm{d}t\, O_\gamma(t) &= \lim_{\tau\to\infty}\frac{1}{\tau}\int_0^\tau \mathrm{d}t\, \mathrm{e}^{iHt}O_\gamma \mathrm{e}^{-iHt} \\ &= \sum_{m,n}(O_\gamma)_{mn}\,|m\rangle\langle n| \lim_{\tau\to\infty}\frac{1}{\tau}\int_0^\tau \mathrm{d}t\, \mathrm{e}^{i(\epsilon_m-\epsilon_n)t} \\ &= \sum_{\substack{n,m\\ \epsilon_n=\epsilon_m}}(O_\gamma)_{mn}\,|m\rangle\langle n| \end{aligned} \tag{4.5}$$

This time-averaging amounts to a cut-off, removing all matrix elements between non-degenerate eigenstates of the Hamiltonian. A crucial property of this operation is that it is an orthogonal projection in the space of operators, i.e. $\left(\bar{O}_\gamma\middle|\bar{O}_{\gamma'}\right) = \left(\bar{O}_\gamma\middle|O_{\gamma'}\right)$. This will in the end will allow us to distinguish between different types of conserved quantities. However, our ultimate goal concerns LSROs in a system that is not integrable, which dictates the need for performing also a finite-time averaging. Unfortunately, a simple omission of the limit in Eq. (4.5) destroys the projective character of this operation. To remedy this, we introduce a parameter τ and define effective time averaging [137] as

$$\bar{O}^\tau_\gamma = \int_{-\infty}^{\infty}\mathrm{d}t\, O_\gamma(t)\frac{\sin(t/\tau)}{\pi t} \tag{4.6}$$

By considering the Fourier transform of the $\sin(x)/x$ function, it can be shown that this expression is equivalent to (see Appendix C for details)

$$\bar{O}^\tau_\gamma = \sum_{n,m}\underbrace{\theta\left(\frac{1}{\tau}-|\epsilon_n-\epsilon_m|\right)}_{\theta^\tau_{nm}}(O_\gamma)_{mn}\,|m\rangle\langle n| \tag{4.7}$$

and because for Heaviside theta function we have $\theta(x)^2=\theta(x)$, the projective character is restored. Properties the θ-function ensure that the $\tau\to\infty$ limit of Eq. (4.7) agrees with Eq. (4.5). Notice also the similarity of this expression to the integrated conductivity (3.5). Indeed, the parameter $1/\tau$ can be interpreted as Ω, giving the frequency cut-off for the matrix elements. Thus, for finite τ, $\left(\bar{O}^\tau_\gamma\middle|\bar{O}^\tau_{\gamma'}\right)$ can be related to the low-frequency spectrum of the correlation function $\langle O_\gamma(t)O_{\gamma'}\rangle$. We shall return to this idea later on.

Let us now calculate the commutator of O^τ_γ with the Hamiltonian

$$\begin{aligned}\left[H,\bar{O}^\tau_\gamma\right] &= \sum_n\sum_{k,p}\epsilon_n\theta^\tau_{kp}(\bar{O}_\gamma)_{kp}[|n\rangle\langle n|\,,|k\rangle\langle p|] \\ &= \sum_{k,p}(\epsilon_k-\epsilon_p)\,\theta^\tau_{kp}(\bar{O}_\gamma)_{kp}\,|k\rangle\langle p| \xrightarrow{\tau\to\infty} 0\end{aligned} \tag{4.8}$$

We see that the operator obtained from infinite-time averaging is an integral of motion. Unfortunately, this procedure modifies the support of the operator and in general $\bar{O}_\gamma\notin\mathcal{V}_M$, i.e. its locality is lost.

Having calculated the time-averaged basis $\{\bar{O}^\tau_\gamma\}$, we would like to perform in a systematic way the decomposition 4.4. We need the overlaps between the basis operators before and after the time-averaging. Because of the projective character of the time-averaging, they are given by the pairwise inner products of the time-averaged operators, which we collect into a matrix K^τ, with elements

$$K^\tau_{\gamma\gamma'} = \left(\bar{O}^\tau_\gamma\middle|\bar{O}^\tau_{\gamma'}\right) = \frac{1}{\mathcal{D}}\sum_{n,m}\theta^\tau_{nm}(O_\gamma)_{nm}(O_{\gamma'})^*_{nm} \tag{4.9}$$

This matrix is Hermitian by design, and in the case of systems with time-reversal symmetry, it is also real, thus symmetric. By the spectral theorem, there exists a unitary matrix U^τ that transforms it via a similarity transformation to a diagonal matrix D^τ

$$\sum_{\gamma,\gamma'} U^\tau_{\beta\gamma} K^\tau_{\gamma\gamma'} (U^\tau)^*_{\beta'\gamma'} = \delta_{\beta\beta'} \lambda^\tau_\beta \in \mathbb{R}, \quad \lambda_\beta \text{ — eigenvalue of } K^\tau \tag{4.10}$$

$$U^\tau (U^\tau)^\dagger = (U^\tau)^\dagger U^\tau = \mathbb{1} \implies \sum_\gamma (U^\tau)_{\beta\gamma} (U^\tau)^*_{\beta'\gamma} = \delta_{\beta\beta'} \tag{4.11}$$

$$U^\tau K^\tau = D^\tau U^\tau \implies \sum_\gamma U^\tau_{\beta\gamma} K^\tau_{\gamma\gamma'} = \sum_\gamma \delta_{\beta\gamma} \lambda^\tau_\gamma U^\tau_{\gamma\gamma'} = \lambda^\tau_\beta U^\tau_{\beta\gamma'} \tag{4.12}$$

Using the columns of U^τ, which are just the eigenvectors of K^τ, we can construct a new set of operators

$$Q^\tau_\beta = \sum_\gamma U^\tau_{\beta\gamma} \bar{O}^\tau_\gamma \tag{4.13}$$

Let us note a few properties of the newly defined quantities. First, they are orthogonal

$$\begin{aligned} \left(Q^\tau_\beta \middle| Q^\tau_{\beta'}\right) &= \sum_{\gamma,\gamma'} U^\tau_{\beta\gamma} \left(\bar{O_\gamma}^\tau \middle| \bar{O_{\gamma'}}^\tau\right) (U^\tau)^*_{\beta'\gamma'} = \sum_{\gamma'} \left(\sum_\gamma U^\tau_{\beta\gamma} K^\tau_{\gamma\gamma'} \right) (U^\tau)^*_{\beta'\gamma'} \\ &= \lambda^\tau_\beta \sum_{\gamma'} U^\tau_{\beta\gamma'} (U^\tau)^*_{\beta'\gamma'} = \lambda^\tau_\beta \delta_{\beta\beta'} \end{aligned} \tag{4.14}$$

where the last two equalities follow from (4.12) and (4.11) respectively. From the fact that $\left(Q^\tau_\beta \middle| Q^\tau_\beta\right) = \lambda^\tau_\beta$ and that $(\cdot|\cdot)$ is an inner product, we immediately deduce that K^τ is positive semidefinite. We are now ready to consider the desired decomposition into the part that is supported on at most M sites and the remaining, nonlocal part

$$\begin{aligned} Q^\tau_\beta &= \sum_\gamma \left(O_\gamma \middle| Q^\tau_\beta\right) O_\gamma + (Q^\tau_\beta)^\perp = \sum_{\gamma,\gamma'} U^\tau_{\beta\gamma'} \left(O_\gamma \middle| \bar{O}^\tau_{\gamma'}\right) O_\gamma + (Q^\tau_\beta)^\perp \\ &= \sum_{\gamma,\gamma'} U^\tau_{\beta\gamma'} \left(\bar{O}^\tau_\gamma \middle| \bar{O}^\tau_{\gamma'}\right) O_\gamma + (Q^\tau_\beta)^\perp = \sum_{\gamma,\gamma'} U^\tau_{\beta\gamma'} K^\tau_{\gamma\gamma'} O_\gamma + (Q^\tau_\beta)^\perp \\ &= \sum_\gamma \left(\sum_{\gamma'} U^\tau_{\beta\gamma'} K^\tau_{\gamma\gamma'} \right) O_\gamma + (Q^\tau_\beta)^\perp = \sum_\gamma \lambda^\tau_\beta U^\tau_{\beta\gamma} O_\gamma + (Q^\tau_\beta)^\perp = (Q^\tau_\beta)^M + (Q^\tau_\beta)^\perp \end{aligned} \tag{4.15}$$

Everything we did so far holds for an arbitrary value of τ. However, let us for a moment restrict it to $\tau \to \infty$, dropping the superscript. This guarantees that the operators Q_β are integrals of motion. We have one step left to complete the algorithm and obtain a classification scheme for the integrals of motion. We need to determine how much of the operator Q_n is contained in the M-local part Q^M_β. In other words, we want to calculate $\|Q^\perp_\beta\|$. Consider the following calculation

$$\begin{aligned} \lambda_\beta = (Q_\beta|Q_\beta) &= \left(Q^M_\beta + Q^\perp_\beta \middle| Q^M_\beta + Q^\perp_\beta\right) = \left(Q^M_\beta \middle| Q^M_\beta\right) + \left(Q^\perp_\beta \middle| Q^\perp_\beta\right) + \underbrace{2\left(Q^M_\beta \middle| Q^\perp_\beta\right)}_{=0} \\ &= \left(\sum_\gamma \lambda_\beta U_{\beta\gamma} O_\gamma \middle| \sum_{\gamma'} \lambda_\beta U_{\beta\gamma'} O_{\gamma'} \right) + \left\| Q^\perp_\beta \right\|^2 = \lambda^2_\beta \sum_{\gamma,\gamma'} U_{\beta\gamma} \left(O_\gamma | O_{\gamma'}\right) U^*_{\beta\gamma'} + \left\| Q^\perp_\beta \right\|^2 \\ &= \lambda^2_\beta + \left\| Q^\perp_\beta \right\|^2 \end{aligned} \tag{4.16}$$

Rearranging the terms, we obtain the desired formula

$$\left\|Q_\beta^\perp\right\|^2 = \lambda_\beta^2 - \lambda_\beta = \lambda_\beta(\lambda_\beta - 1) \geq 0 \tag{4.17}$$

Thus, the spectrum of the matrix K is contained in the interval $[0, 1]$ and determines the classification of the integrals of motion. We have three classes:

- local: $\lambda_\beta = 1 \implies \left\|Q_\beta^\perp\right\| = 0 \implies Q_\beta \in \mathcal{V}_M$
- quasilocal: $\lambda_\beta \in (0, 1) \implies \left\|Q_\beta^\perp\right\| > 0 \implies Q_\beta \in \mathcal{V}$
- generic nonlocal: $\lambda_\beta = 0 \implies \|Q_\beta\| = 0$

Let us now give a physical interpretation of these results. The procedure outlined above can be carried out for, in principle, arbitrary but finite systems size L. However, to understand the character of the integrals of motion, we need to take the thermodynamic limit $L \to \infty$. In practical calculations, we are always limited to finite, M-local basis of operators. Thus, the output of the algorithm is not the set of true integrals of motion $\{Q_\beta\}$, but rather the set $\{Q_\beta^M/\lambda_n\} \equiv \{I_\beta\}$ (as eigenvectors obtained from numerical procedures are usually normalized). If a particular $\lambda_\beta = 1$, this is not a problem, as we have $\|Q_\beta^M\| = 1$, and the true LIOM is M-local. However, if for a given β we have $0 < \lambda_\beta < 1$, then $\|Q_\beta^M\| < 1$. It is only if this norm stays non-zero in the thermodynamic limit, we can say that the operator is quasilocal. Then the Q_β^M can be regarded as an M-local approximation of the true LIOM Q_β. Numerous studies have confirmed their relevance in the theory of integrable systems [138–141], however, we shall not deal with them any further. In fact, we shall not even deal with LIOMs, as the system we are interested in here is not integrable. Nevertheless, even without integrability, this algorithm will produce a sequence of operators $\{I_\beta\}$, with the largest possible norm, often called **stiffness**. We will refer to them as **local slowly relaxing operators (LSROs)** and they will play a central role in section 4.2. We shall also relax the restriction $\tau \to \infty$ and look at the LSROs at finite values of τ.

4.1.2 Details of implementation

Before proceeding further toward a concrete application of the procedure outlined above, let us first discuss some technical details of its implementation. The most demanding part, from the computational point of view, is the calculation of matrix elements (4.9). It requires explicit construction of matrices of all the basis operators O_γ, change of basis using Hamiltonian eigenstates, time averaging (4.7), and finally carrying out the trace of pairwise products. All those operations are constrained by the fact that the Hilbert space dimension grows exponentially. To keep the computational cost manageable, we can use symmetries of the system. In chapter 1, we have explored how the presence of a symmetry, manifested by the existence of an operator S, such that $[S, H] = 0$, can be used to decompose the Hilbert space into a direct sum of $s_{\max}$ smaller subspaces $\mathcal{H}_s$, consisting of states with a fixed eigenvalue s of S. Given a compatible operator A, its matrix in the symmetry-adapted basis has a block-diagonal structure. It is easy to see that then, its trace is equal to the sum of traces of the individual blocks. Thus, instead of carrying out the algorithm in the full Hilbert space,

we can perform it separately in each symmetry sector and then construct the matrix K^τ by summing the matrices of the individual sectors. However, there is a caveat. We require the basis operators O_γ to be traceless, to avoid trivial overlaps with the identity operator, and normalized, to form an orthonormal basis. But they must be traceless and normalized with respect to the full space Hilbert-Schmidt inner product (4.2), not the one restricted to a symmetry sector. It is known from linear algebra, that given a collection of spaces equipped with an inner product, a unique way to define an inner product on the direct sum of those spaces is to consider the sum of the individual inner products [142]. Thus, we have the following identities

$$\Lambda_A \equiv \frac{1}{\mathcal{D}} \operatorname{Tr}(A) = \frac{1}{\mathcal{D}} \sum_{s=1}^{s_{\max}} \operatorname{Tr}(A^s) \tag{4.18}$$

$$\Gamma_A \equiv \|A\|^2 = \frac{1}{\mathcal{D}} \operatorname{Tr}\left(A^\dagger A\right) = \frac{1}{\mathcal{D}} \sum_{s=1}^{s_{\max}} \operatorname{Tr}\left((A^s)^\dagger A^s\right) \tag{4.19}$$

where by A^s we denote the block of matrix of A in the symmetry sector with eigenvalue s. Now, we are ready to derive the formula for the overlap matrix, using symmetry sectors. For brevity, we shall suppress the τ superscript.

$$\begin{aligned} K_{\gamma\gamma'} &= \left(\frac{\bar{O}_\gamma - \Lambda_{O_\gamma}}{\Gamma_{O_\gamma}} \middle| \frac{\bar{O}_{\gamma'} - \Lambda_{O_{\gamma'}}}{\Gamma_{O_{\gamma'}}} \right) = \frac{1}{\mathcal{D}} \operatorname{Tr} \left(\frac{\bar{O}_\gamma - \Lambda_{O_\gamma}}{\Gamma_{O_\gamma}} \frac{\bar{O}_{\gamma'} - \Lambda_{O_{\gamma'}}}{\Gamma_{O_{\gamma'}}} \right) \\ &= \frac{1}{\mathcal{D}\Gamma_{O_\gamma}\Gamma_{O_{\gamma'}}} \left[\operatorname{Tr}\left(\bar{O}_\gamma \bar{O}_{\gamma'}\right) - \Lambda_{\gamma'} \operatorname{Tr}(O_\gamma) - \Lambda_\gamma \operatorname{Tr}(O_{\gamma'}) + \Lambda_\gamma \Lambda_{\gamma'} \mathcal{D} \right] \\ &= \frac{1}{\mathcal{D}\Gamma_{O_\gamma}\Gamma_{O_{\gamma'}}} \left[\operatorname{Tr}\left(\bar{O}_\gamma \bar{O}_{\gamma'}\right) - \Lambda_{\gamma'} \Lambda_\gamma \mathcal{D} \right] \\ &= \frac{1}{\mathcal{D}\Gamma_{O_\gamma}\Gamma_{O_{\gamma'}}} \left[\sum_{s=1}^{s_{\max}} \operatorname{Tr}\left(\bar{O}^s_\gamma \bar{O}^s_{\gamma'}\right) - \Lambda_{\gamma'} \Lambda_\gamma \mathcal{D} \right] \end{aligned} \tag{4.20}$$

Algorithm 5 summarizes the procedure for finding LIOMs/LSROs, optimized using symmetry subspaces.

There is one more possible improvement to the algorithm. We have spent the better part of chapter 2 developing numerical methods that allow us to avoid using exact diagonalization. However, the algorithm presented above requires knowledge of the full eigenspectrum of the Hamiltonian. It turns out, that it is possible to escape this requirement, and instead rely on the Dynamical Quantum Typicality approach to correlation functions. We have already hinted at that relationship after introducing finite time averaging (4.7). To see this, let us calculate the Fourier transform of an infinite-temperature correlation function between two operators A and B. It is a bit lengthy to carry out the calculation in a rigorous way, so the details are relegated to Appendix C. The result, written in spectral representation, is

$$\mathcal{F}\left[(A(t)|B)\right] = \frac{1}{\mathcal{D}} \sum_{n,m} A_{mn} B_{nm} \delta(\epsilon_m - \epsilon_n + \omega) \tag{4.21}$$

Let us now do one more step and consider the integral of $\mathcal{F}\left[(A(t)|B)\right]$ over some finite

frequency window $[-\Omega, \Omega]$, akin to the integrated conductivity (3.5).

$$\begin{aligned}\mathcal{I}_{AB}(\Omega) &= \int_{-\Omega}^{\Omega} \mathrm{d}\omega\ \mathcal{F}\left[(A(t)|B)\right](\omega) = \frac{1}{\mathcal{D}} \sum_{n,m} A_{mn} B_{nm} \int_{-\Omega}^{\Omega} \mathrm{d}\omega\ \delta(\epsilon_m - \epsilon_n + \omega) \\ &= \frac{1}{\mathcal{D}} \sum_{n,m} A_{mn} B_{nm} \theta(\Omega + (\epsilon_m - \epsilon_n)) \theta(\Omega - (\epsilon_m - \epsilon_n)) \\ &= \frac{1}{\mathcal{D}} \sum_{n,m} A_{mn} B_{nm} \theta(\Omega - |\epsilon_m - \epsilon_n|) \end{aligned} \tag{4.22}$$

This is a very important result, and the quantity $\mathcal{I}_{AB}(\Omega)$ goes by the name of the integrated spectral function [143]. It tells us that the matrix element of the overlap matrix K^τ, for a pair of operators A and B, is equal to the integrated Fourier transform of the infinite-temperature correlation function between A and B. This means that we can calculate the matrix elements of K^τ by using the Dynamical Quantum Typicality and Lanczos-based approach, which should be more efficient than exact diagonalization. Unfortunately, this is not the case for the physical system considered in this thesis, i.e. the long-range Heisenberg model. The reason is that the efficiency of Lanczos-based correlation function calculation relies on the sparse structure of the Hamiltonian matrix. This is of course not the case for a power-law decaying interaction. Thus, we will not use this approach here, as its performance is worse than exact diagonalization. However, all the work is not in vain, as this method will surely prove useful for further research.

4.2 Fermionic currents in the long-range Heisenberg model

We are now ready to apply the algorithm described in the previous section to the long-range Heisenberg model. Let us stress again, that this model is not integrable, thus we do not expect to find any strictly conserved, local operator, i.e. LIOMs I_β with $\lambda_\beta = 1$. Nevertheless, we can still hope to find a sequence of operators with large stiffness, indicating their slow relaxation.

In order to use the procedure, we need to construct a basis of the operator space $\mathcal{V}_M$. Our starting point is a set of traceless, translationally invariant operators $\{O'_\gamma\}$,

$$O'_\gamma = \frac{1}{\sqrt{L}} \sum_{\ell=1}^{L} (o_{\ell+1} o_{\ell+2} \dots o_{\ell+M}) \tag{4.23}$$

where $o_\ell \in \{\mathbb{1}_\ell, \sqrt{2}S^-_\ell, \sqrt{2}S^+_\ell, 2S^z_\ell\}$ are the single-site operators. It can be verified by direct calculation that they are orthonormal with respect to the Hilbert-Schmidt inner product, as required. However, they are not Hermitian. We have two possible ways to remedy this. First, is to consider **real operators** of the form $O_\gamma = (O'_\gamma + {O'_\gamma}^\dagger)$. The Hamiltonian (1.2) is an example of a real operator. The second option is to consider **imaginary operators**, defined as $O_\gamma = i(O'_\gamma - {O'_\gamma}^\dagger)$. The spin current (1.13) belongs to this class. Fortunately, operators belonging to different classes are orthogonal, so we can consider them separately. Here, we are seeking the most conserved operators, sharing some properties with the spin current, so we are going to focus on the imaginary operators. We numerically perform the steps described in Algorithm 5, initially for $\tau \to \infty$, using the basis of imaginary operators $\{O_\gamma\}$ and the Hamiltonian (1.2) and obtain a sequence of local, orthonormal observables $I_\beta = \sum_\gamma U_{\beta\gamma} O_\gamma$

Algorithm 5 Algorithm for finding LIOMs/LSROs, optimized using symmetry subspaces

Input: $\{O_i\}_{i=1}^N$ — Basis of the operator space $\mathcal{V}_M$, tight-binding Hamiltonian H

Output: $\{I_i\}_{i=1}^N$ — most conserved operators (LIOMs/LSROs)

$\Gamma_{O_i} = 0$, $\Lambda_{O_i} = 0$, $K_{ij} = 0$ for all $i, j = 1, \dots N$
for $s = 1 : s_{\max}$ **do**
    Generate and diagonalize H^s
    for $i = 1 : N$ **do**
        Generate O_i^s
        $\Gamma_{O_i} = \Gamma_{O_i} + \frac{1}{\mathcal{D}} \operatorname{Tr}\left((O_i^s)^\dagger O_i^s\right)$
        $\Lambda_{O_i} = \Lambda_{O_i} + \frac{1}{\mathcal{D}} \operatorname{Tr}(O_i^s)$
        Change basis and calculate $\bar{O}_i^s$ according to Eq. (4.7)
        for $j = i : N$ **do**
            Generate O_j^s, calculate $\bar{O}_j^s$ according to Eq. (4.7)
            $K_{ij} = K_{ij} + \frac{1}{\mathcal{D}} \operatorname{Tr}\left(\bar{O}_i^s \bar{O}_j^s\right)$
            $K_{ji} = K_{ji} + (1 - \delta_{ij}) K_{ij}$
        end for
    end for
end for
for $i, j = 1 : N$ **do**
    $K_{ij} = K_{ij} - \mathcal{D} \Lambda_{O_i} \Lambda_{O_j}$
    $K_{ij} = K_{ij} / (\mathcal{D} \Gamma_{O_i} \Gamma_{O_j})$
end for
Diagonalize K, obtaining eigenvalues $\{\lambda_i\}$ and eigenvectors $\{U_{ij}\}$
$\{Q_i^M\} = \sum_j U_{ij} O_j$

together with corresponding stiffnesses λ_β. Figure 4.1 shows the stiffness of the top 3 operators, on the parameters Δ and γ. These results were obtained for a system of $L = 14$ sites, with a maximal operator support of $M = 4$.

Heatmaps of stiffness

Figure 4.1: Heatmaps depicting the dependence of the stiffness of the top 3 operators on the parameters Δ and γ. From left to right we have λ_1, λ_2 and λ_3 respectively. The black line corresponds to the optimal anisotropy $\Delta_O(\alpha) = \exp(-\alpha + 2)$.

We see that λ_2 and λ_3 exhibit behavior resembling the initially investigated spin current, that is a clear maximum along the line of optimal anisotropy $\Delta_O(\alpha) = \exp(-\alpha + 2)$, whereas λ_1 is approximately constant above this line and sharply drops below it. As we are not aware of any mechanics explaining non-zero stiffness in the thermodynamic limit, we have also carried out a finite-size analysis of operators I_2 and I_3 for 3 points in the parameter space: below the optimal line $(\alpha, \Delta) = (3.5, 0.0)$, on the optimal line $(\alpha, \Delta) = (3.5, 0.2)$ and above the optimal line $(\alpha, \Delta) = (3.5, 0.8)$. The results are shown in Figure 4.2.

Finite size analysis

Figure 4.2: Finite size dependence of λ_2 (left panel) and λ_3 (right panel) for the optimal anisotropy $\alpha = 3.5$, $\Delta = 0.2$ and away from it ($\Delta = 0.0, 0.8$).

We observe another feature manifesting itself along the line of optimal anisotropy. Not only the stiffness is the largest, but its dependence on the system size is also the weakest. Still, we know of no reason for it to stay finite in the thermodynamic limit, so we expect it to decay for systems much beyond our reach.

To learn more about the nature of the operators I_1, I_2, and I_3, we have also examined the contribution of each basis operator O_γ to their structure. Specifically, we have calculated the projections $(O_\gamma|I_\beta)^2 = |U_{\gamma\beta}|^2$ and discovered that the largest contributions come from three imaginary (current-like) operators

$$\begin{aligned} O_1 &= i\frac{2}{\sqrt{L}}\sum_{\ell=1}^{L}\left(S^+_\ell S^-_{\ell+1} - \text{H.c.}\right) \\ O_2 &= i\frac{4}{\sqrt{L}}\sum_{\ell=1}^{L}\left(S^+_\ell S^z_{\ell+1} S^+_{\ell+2} - \text{H.c.}\right) \\ O_3 &= i\frac{8}{\sqrt{L}}\sum_{\ell=1}^{L}\left(S^+_\ell S^z_{\ell+1} S^z_{\ell+2} S^+_{\ell+3} - \text{H.c.}\right) \end{aligned} \tag{4.24}$$

The adjective *fermionic* describing these currents stems from their image under Jordan-Wigner transformation, namely currents describing particle hopping between first-, second-, and third-nearest neighbors in a system of spinless fermions. The dependence of the projections on the parameters is shown in Figure 4.3.

We see that the best LSRO, I_1, has nonzero overlap only with O_2, which is even under the spin-flip transformation[2]. Both O_1 and O_3 are odd under this transformation, so they do not

[2]Spin-flip transformation maps S^z_ℓ to $-S^z_\ell$. S^+_ℓ to S^-_ℓ and S^-_ℓ to S^+_ℓ.

Heatmaps of projections

Figure 4.3: Projections of the LSROs I_β on the local operators O_γ defined in (4.24), i.e. $(O_\gamma|I_\beta)^2 = |U_{\gamma\beta}|^2$ for $\beta = 1, 2, 3$ and $\gamma = 1, 2, 3$.

contribute to I_1. This is a consequence of the orthogonality between even and odd subspaces of operator space $\mathcal{V}_\mathrm{M}$ and in fact those two spaces can be considered separately to reduce the computational cost. Observing that $\lambda_1 \to 1$ as $\alpha \to \infty$ and $(O_2|I_1)^2 \to 1$ as $\Delta \to 0$, we can suspect that this LSRO is a remnant of the energy current operator [66], which in the nearest-neighbor Heisenberg model is a proper LIOM. Next, I_2 has a nonzero overlap only with O_1 and O_3, which are odd under spin flip. Moreover, the overlap $(O_1|I_2)^2$ is maximal along the line of optimal anisotropy. Similar behavior is observed for I_3, but now the overlap with O_3 is maximal along the line. However, there is a slight difference in comparison to the previous two LSROs. There are values of parameters for which I_3 has overlap with just the odd currents, whereas for others only with the even one. This is caused by the fact the I_3, defined as the operator with the third largest stiffness, can have a completely different structure depending on the parameters of the model. Nevertheless, the important fact is that for optimal anisotropy, it is the odd current that contributes the most. It is an interesting fact that even though this model cannot be mapped onto a fermionic system with two-body interactions, numerical evidence points to the existence of long-lived local, fermionic currents which are the most stable at the line of optimal anisotropy.

Finally, we consider the case $\tau < \infty$ and look at the eigenvalues of the overlap matrix K^τ as functions of $\Omega = 1/\tau$. Let us stop for a moment and see another interpretation of the eigenvalues of K^τ

$$\begin{aligned}
\lambda^\tau_\beta &= \left(Q^\tau_\beta \middle| Q^\tau_\beta\right) = \sum_{\gamma\gamma'} U_{\beta\gamma} \left(\bar{O}^\tau_\gamma \middle| \bar{O}^\tau_{\gamma'}\right) U^*_{\beta\gamma'} \\
&= \frac{1}{\mathcal{D}} \sum_{\gamma\gamma'} \sum_{n,m} \theta^\tau_{nm} \left(O_\gamma\right)_{nm} \left(O_{\gamma'}\right)_{mn} U_{\beta\gamma} U^*_{\beta\gamma'} \\
&= \frac{1}{\mathcal{D}} \sum_{n,m} \theta^\tau_{mn} \underbrace{\left[\sum_\gamma U_{\beta\gamma} \left(O_\gamma\right)_{nm}\right]}_{} \left(I_\beta\right)_{nm} \underbrace{\left[\sum_{\gamma'} U^*_{\beta\gamma'} \left(O_{\gamma'}\right)_{mn}\right]}_{} \left(I_\beta\right)^*_{mn} \\
&= \frac{1}{\mathcal{D}} \sum_{n,m} \theta^\tau_{nm} \left|\left(I_\beta\right)_{nm}\right|^2 = \mathcal{I}_{I_\beta I_\beta}\left(\frac{1}{\tau}\right)
\end{aligned} \tag{4.25}$$

This is precisely the integrated spectral function (4.22) of the operator I_β at frequency $\Omega = 1/\tau$. Thus, by investigating the eigenvalues of K^τ we can study our LSROs on the same footing as the integrated conductivity in the previous chapter. Ω-dependence of the eigenvalues of K^τ for the 3 operators with largest stiffnesses, I_1, I_2, and I_3, is shown in Figure 4.4.

Eigenvalues of K^τ for the 3 operators with largest stiffnesses

Figure 4.4: Eigenvalues of K^τ for the 3 operators with largest stiffnesses, I_1, I_2, and I_3, as a function of $\Omega = 1/\tau$.

5 Summary

AAA

Bibliography

[1] K. Huang, *Statistical Mechanics* (Wiley, 1987).

[2] R. P. Feynman, *Statistical mechanics: A set of lectures*, Advanced Books Classics (Avalon Publishing, 2018).

[3] L. D. Landau and E. M. Lifshitz, *Mechanics* (1976).

[4] J. J. Sakurai and J. Napolitano, *Modern Quantum Mechanics* (Cambridge University Press, Sept. 2017).

[5] S. Trotzky, Y.-A. A. Chen, A. Flesch, I. P. McCulloch, U. Schollwöck, J. Eisert, and I. Bloch, "Probing the relaxation towards equilibrium in an isolated strongly correlated one-dimensional Bose gas", Nat. Phys. **8**, 325–330 (2012).

[6] M. Rigol and M. Srednicki, "Alternatives to eigenstate thermalization", Phys. Rev. Lett. **108**, 110601 (2012).

[7] M. Rigol, V. Dunjko, and M. Olshanii, "Thermalization and its mechanism for generic isolated quantum systems", Nature **452**, 854–858 (2008).

[8] C. L. Hung, X. Zhang, N. Gemelke, and C. Chin, "Slow mass transport and statistical evolution of an atomic gas across the superfluid-mott-insulator transition", Phys. Rev. Lett. **104**, 160403 (2010).

[9] S. Hofferberth, I. Lesanovsky, B. Fischer, T. Schumm, and J. Schmiedmayer, "Non-equilibrium coherence dynamics in one-dimensional Bose gases", Nature **449**, 324–327 (2007).

[10] P. W. Shor, "Scheme for reducing decoherence in quantum computer memory", Phys. Rev. A **52**, 2493–2496 (1995).

[11] R. J. Lewis-Swan, A. Safavi-Naini, A. M. Kaufman, and A. M. Rey, "Dynamics of quantum information", Nature Reviews Physics **1**, 627–634 (2019).

[12] E. R. MacQuarrie, C. Simon, S. Simmons, and E. Maine, "The emerging commercial landscape of quantum computing", Nature Reviews Physics **2**, 596–598 (2020).

[13] J. M. Deutsch, "Quantum statistical mechanics in a closed system", Phys. Rev. A **43**, 2046–2049 (1991).

[14] M. Srednicki, "Chaos and quantum thermalization", Phys. Rev. E **50**, 888–901 (1994).

[15] E. P. Wigner, "Characteristic Vectors of Bordered Matrices With Infinite Dimensions", The Annals of Mathematics **62**, 548 (1955).

[16] V. L. Girko, *Random matrices*, Vol. 1, ISSN (Elsevier Science, 1996), pp. 27–78.

[17] L. D'Alessio, Y. Kafri, A. Polkovnikov, and M. Rigol, "From quantum chaos and eigenstate thermalization to statistical mechanics and thermodynamics", Adv. Phys. **65**, 239–362 (2016).

[18] W. Beugeling, R. Moessner, and M. Haque, "Finite-size scaling of eigenstate thermalization", Phys. Rev. E **89**, 042112 (2014).

[19] J. M. Magán, "Random Free Fermions: An Analytical Example of Eigenstate Thermalization", Phys. Rev. Lett. **116**, 030401 (2016).

[20] L. F. Santos and M. Rigol, "Onset of quantum chaos in one-dimensional bosonic and fermionic systems and its relation to thermalization", Phys. Rev. E **81**, 036206 (2010).

[21] M. Rigol and L. F. Santos, "Quantum chaos and thermalization in gapped systems", Phys. Rev. A **82**, 011604 (2010).

[22] E. Khatami, G. Pupillo, M. Srednicki, and M. Rigol, "Fluctuation-dissipation theorem in an isolated system of quantum dipolar bosons after a quench", Phys. Rev. Lett. **111**, 050403 (2013).

[23] M. Rigol, "Breakdown of Thermalization in Finite One-Dimensional Systems", Phys. Rev. Lett. **103**, 100403 (2009).

[24] C. Neuenhahn and F. Marquardt, "Thermalization of interacting fermions and delocalization in Fock space", Phys. Rev. E **85**, 060101 (2012).

[25] M. Rigol, "Quantum quenches and thermalization in one-dimensional fermionic systems", Phys. Rev. A **80**, 053607 (2009).

[26] C. J. Turner, A. A. Michailidis, D. A. Abanin, M. Serbyn, and Z. Papić, "Quantum scarred eigenstates in a Rydberg atom chain: Entanglement, breakdown of thermalization, and stability to perturbations", Phys. Rev. B **98**, 155134 (2018).

[27] C. J. Turner, A. A. Michailidis, D. A. Abanin, M. Serbyn, and Z. Papić, "Weak ergodicity breaking from quantum many-body scars", Nat. Phys. **14**, 745–749 (2018).

[28] F. Wilczek, "Quantum Time Crystals", Phys. Rev. Lett. **109**, 160401 (2012).

[29] K. Sacha and J. Zakrzewski, "Time crystals: a review", Rep. Prog. Phys. **81**, 016401 (2017).

[30] D. M. Basko, I. L. Aleiner, and B. L. Altshuler, "Metal–insulator transition in a weakly interacting many-electron system with localized single-particle states", Ann. Phys. **321**, 1126–1205 (2006).

[31] S. Dal Conte, L. Vidmar, D. Golež, M. Mierzejewski, G. Soavi, S. Peli, F. Banfi, G. Ferrini, R. Comin, B. M. Ludbrook, L. Chauviere, N. D. Zhigadlo, H. Eisaki, M. Greven, S. Lupi, A. Damascelli, D. Brida, M. Capone, J. Bonča, G. Cerullo, and C. Giannetti, "Snapshots of the retarded interaction of charge carriers with ultrafast fluctuations in cuprates", Nat. Phys. **11**, 421–426 (2015).

[32] J. S. Caux and J. Mossel, "Remarks on the notion of quantum integrability", J. Stat. Mech: Theory Exp. **2011**, P02023 (2011).

[33] E. A. Yuzbashyan and B. S. Shastry, "Quantum Integrability in Systems with Finite Number of Levels", J. Statist. Phys. **150**, 704–721 (2013).

[34] L. D. Faddeev, "Algebraic Aspects of the Bethe Ansatz", Int. J. Modern Phys. A **10**, 1845–1878 (1995).

[35] L. D. Faddeev, "How Algebraic Bethe Ansatz works for integrable model", Fifty Years of Mathematical Physics, 370–439 (1996).

[36] V. E. Korepin, N. M. Bogoliubov, and A. G. Izergin, *Quantum Inverse Scattering Method and Correlation Functions* (Cambridge University Press, Aug. 1993).

[37] U. Agrawal, S. Gopalakrishnan, R. Vasseur, and B. Ware, "Anomalous low-frequency conductivity in easy-plane XXZ spin chains", Phys. Rev. B **101**, 224415 (2020).

[38] A. J. Friedman, S. Gopalakrishnan, and R. Vasseur, "Diffusive hydrodynamics from integrability breaking", Phys. Rev. B **101**, 180302 (2020).

[39] B. Bertini, F. Heidrich-Meisner, C. Karrasch, T. Prosen, R. Steinigeweg, and M. Žnidarič, "Finite-temperature transport in one-dimensional quantum lattice models", Rev. Mod. Phys. **93**, 1–71 (2021).

[40] A. Bastianello, A. D. Luca, and R. Vasseur, "Hydrodynamics of weak integrability breaking", J. Stat. Mech: Theory Exp. **2021**, 114003 (2021).

[41] V. B. Bulchandani, S. Gopalakrishnan, and E. Ilievski, "Superdiffusion in spin chains", J. Stat. Mech: Theory Exp. **2021**, 084001 (2021).

[42] V. Khemani, C. R. Laumann, and A. Chandran, "Signatures of integrability in the dynamics of Rydberg-blockaded chains", Phys. Rev. B **99**, 161101 (2019).

[43] A. Browaeys and T. Lahaye, "Many-body physics with individually controlled rydberg atoms", Nat. Phys. **16**, 132–142 (2020).

[44] X. Zotos, "High temperature thermal conductivity of two-leg spin-1/2 ladders", Phys. Rev. Lett. **92**, 067202 (2004).

[45] G. P. Brandino, J. S. Caux, and R. M. Konik, "Glimmers of a Quantum KAM Theorem: Insights from Quantum Quenches in One-Dimensional Bose Gases", Phys. Rev. X **5**, 041043 (2015).

[46] T. LeBlond, D. Sels, A. Polkovnikov, and M. Rigol, "Universality in the onset of quantum chaos in many-body systems", Phys. Rev. B **104**, L201117 (2021).

[47] J. Sirker, N. P. Konstantinidis, F. Andraschko, and N. Sedlmayr, "Locality and thermalization in closed quantum systems", Phys. Rev. A **89**, 042104 (2014).

[48] L. Campos Venuti and P. Zanardi, "Unitary equilibrations: Probability distribution of the Loschmidt echo", Phys. Rev. A **81**, 022113 (2010).

[49] J. Šuntajs, J. Bonča, T. Prosen, and L. Vidmar, "Ergodicity breaking transition in finite disordered spin chains", Phys. Rev. B **102**, 064207 (2020).

[50] J. Šuntajs and L. Vidmar, "Ergodicity Breaking Transition in Zero Dimensions", Phys. Rev. Lett. **129**, 060602 (2022).

[51] A. Polkovnikov, K. Sengupta, A. Silva, and M. Vengalattore, "Colloquium: Nonequilibrium dynamics of closed interacting quantum systems", Rev. Mod. Phys. **83**, 863–883 (2011).

[52] S. Gopalakrishnan and R. Vasseur, "Anomalous transport from hot quasiparticles in interacting spin chains", Rep. Prog. Phys. **86**, 036502 (2023).

[53] V. I. Arnold, *Mathematical methods of classical mechanics*, Vol. 80, Graduate Texts in Mathematics 1 (Springer New York, 1990).

[54] A. N. Kolmogorov, "On conservation of conditionally periodic motions for a small change in Hamilton's function", Dokl. Akad. Nauk **98**, 527–530 (1954).

[55] V. I. Arnold, "Proof of a Theorem of a. N. Kolmogorov on the Invariance of Quasi-Periodic Motions Under Small Perturbations of the Hamiltonian", Russ. Math. Surv. **18**, 9–36 (2021).

[56] J. Moser, "On invariant curves of area-preserving mappings of an annulus", Nachr. Akad. Wiss. Göttingen Math.-Phys. Kl. II **1962**, 1–20 (1962).

[57] K. Mallayya, M. Rigol, and W. De Roeck, "Prethermalization and Thermalization in Isolated Quantum Systems", Phys. Rev. X **9**, 21027 (2019).

[58] B. Bertini, F. H. Essler, S. Groha, and N. J. Robinson, "Prethermalization and thermalization in models with weak integrability breaking", Phys. Rev. Lett. **115**, 180601 (2015).

[59] J. Berges, S. Borsányi, and C. Wetterich, "Prethermalization", Phys. Rev. Lett. **93**, 142002 (2004).

[60] T. Langen, T. Gasenzer, and J. Schmiedmayer, "Prethermalization and universal dynamics in near-integrable quantum systems", J. Stat. Mech: Theory Exp. **2016**, 064009 (2016).

[61] L. N. Trefethen and D. I. I. I. Bau, *Numerical Linear Algebra* (Philadelphia, 1997).

[62] A. W. Sandvik, "Computational studies of quantum spin systems", AIP Conf. Proc. **1297**, 135–338 (2010).

[63] T. J. Park and J. C. Light, "Unitary quantum time evolution by iterative Lanczos reduction", J. Chem. Phys. **85**, 5870–5876 (1986).

[64] C. Bartsch and J. Gemmer, "Dynamical typicality of quantum expectation values", Phys. Rev. Lett. **102**, 110403 (2009).

[65] C. Sanderson and R. Curtin, "Armadillo: a template-based C++ library for linear algebra", The Journal of Open Source Software **1**, 26 (2016).

[66] X. Zotos, F. Naef, and P. Prelovsek, "Transport and conservation laws", Phys. Rev. B **55**, 11029–11032 (1997).

[67] C. Nisoli, V. Kapaklis, and P. Schiffer, "Deliberate exotic magnetism via frustration and topology", Nat. Phys. **13**, 200–203 (2017).

[68] A. W. Sandvik, "Ground states of a frustrated quantum spin chain with long-range interactions", Phys. Rev. Lett. **104**, 137204 (2010).

[69] L. Yang and A. E. Feiguin, "From deconfined spinons to coherent magnons in an antiferromagnetic heisenberg chain with long range interactions", SciPost Phys. **10**, 10.21468/SCIPOSTPHYS.10.5.111 (2021).

[70] L. Balents, "Spin liquids in frustrated magnets", Nature **464**, 199–208 (2010).

[71] W. S. Bakr, J. I. Gillen, A. Peng, S. Fölling, and M. Greiner, "A quantum gas microscope for detecting single atoms in a Hubbard-regime optical lattice", Nature **462**, 74–77 (2009).

[72] D. Greif, M. F. Parsons, A. Mazurenko, C. S. Chiu, S. Blatt, F. Huber, G. Ji, and M. Greiner, "Site-resolved imaging of a fermionic Mott insulator", Science **351**, 953–957 (2016).

[73] M. F. Parsons, F. Huber, A. Mazurenko, C. S. Chiu, W. Setiawan, K. Wooley-Brown, S. Blatt, and M. Greiner, "Site-Resolved Imaging of Fermionic ^{6}Li in an Optical Lattice", Phys. Rev. Lett. **114**, 213002 (2015).

[74] M. Boll, T. A. Hilker, G. Salomon, A. Omran, J. Nespolo, L. Pollet, I. Bloch, and C. Gross, "Spin- and density-resolved microscopy of antiferromagnetic correlations in Fermi-Hubbard chains", Science **353**, 1257–1260 (2016).

[75] V. Borish, O. Marković, J. Hines, S. Rajagopal, and M. Schleier-Smith, "Transverse-field ising dynamics in a rydberg-dressed atomic gas", Phys. Rev. Lett. **124**, 063601 (2020).

[76] P. Scholl, H. J. Williams, G. Bornet, F. Wallner, D. Barredo, L. Henriet, A. Signoles, C. Hainaut, T. Franz, S. Geier, A. Tebben, A. Salzinger, G. Zürn, T. Lahaye, M. Weidemüller, and A. Browaeys, "Microwave-engineering of programmable xxz hamiltonians in arrays of rydberg atoms", PRX Quantum **3**, 020303 (2022).

[77] S. Hollerith, K. Srakaew, D. Wei, A. Rubio-Abadal, D. Adler, P. Weckesser, A. Kruckenhauser, V. Walther, R. van Bijnen, J. Rui, C. Gross, I. Bloch, and J. Zeiher, "Realizing distance-selective interactions in a rydberg-dressed atom array", Phys. Rev. Lett. **128**, 113602 (2022).

[78] L.-M. Steinert, P. Osterholz, R. Eberhard, L. Festa, N. Lorenz, Z. Chen, A. Trautmann, and C. Gross, "Spatially tunable spin interactions in neutral atom arrays", arXiv:2206.12385 (2022).

[79] S. Geier, N. Thaicharoen, C. Hainaut, T. Franz, A. Salzinger, A. Tebben, D. Grimshandl, G. Zürn, and M. Weidemüller, "Floquet hamiltonian engineering of an isolated many-body spin system", Science **374**, 1149–1152 (2021).

[80] P. Richerme, Z.-X. Gong, A. Lee, C. Senko, J. Smith, M. Foss-Feig, S. Michalakis, A. V. Gorshkov, and C. Monroe, "Non-local propagation of correlations in quantum systems with long-range interactions", Nature **511**, 198–201 (2014).

[81] P. Jurcevic, B. P. Lanyon, P. Hauke, C. Hempel, P. Zoller, R. Blatt, and C. F. Roos, "Quasiparticle engineering and entanglement propagation in a quantum many-body system", Nature **511**, 202–205 (2014).

[82] P. Hauke and L. Tagliacozzo, "Spread of correlations in long-range interacting quantum systems", Phys. Rev. Lett. **111**, 207202 (2013).

[83] M. Foss-Feig, Z.-X. Gong, C. W. Clark, and A. V. Gorshkov, "Nearly linear light cones in long-range interacting quantum systems", Phys. Rev. Lett. **114**, 157201 (2015).

[84] M. F. Maghrebi, Z.-X. Gong, M. Foss-Feig, and A. V. Gorshkov, "Causality and quantum criticality in long-range lattice models", Phys. Rev. B **93**, 125128 (2016).

[85] L. Lepori, A. Trombettoni, and D. Vodola, "Singular dynamics and emergence of nonlocality in long-range quantum models", J. Stat. Mech: Theory Exp. **2017**, 033102 (2017).

[86] I. Frérot, P. Naldesi, and T. Roscilde, "Entanglement and fluctuations in the xxz model with power-law interactions", Phys. Rev. B **95**, 245111 (2017).

[87] L. Vanderstraeten, M. V. Damme, H. P. Büchler, and F. Verstraete, "Quasiparticles in quantum spin chains with long-range interactions", Phys. Rev. Lett. **121**, 090603 (2018).

[88] L. Cevolani, J. Despres, G. Carleo, L. Tagliacozzo, and L. Sanchez-Palencia, "Universal scaling laws for correlation spreading in quantum systems with short- and long-range interactions", Phys. Rev. B **98**, 024302 (2018).

[89] B. Kloss and Y. Bar Lev, "Spin transport in a long-range-interacting spin chain", Phys. Rev. A **99**, 032114 (2019).

[90] J. Ren, W.-L. You, and X. Wang, "Entanglement and correlations in a one-dimensional quantum spin- 12 chain with anisotropic power-law long-range interactions", Phys. Rev. B **101**, 094410 (2020).

[91] V. B. Bulchandani and D. A. Huse, "Hot band sound", arXiv:2208.13767 (2022).

[92] J. P. Ronzheimer, M. Schreiber, S. Braun, S. Hodgman, S. Langer, I. P. McCulloch, F. Heidrich-Meisner, I. Bloch, and U. Schneider, "Expansion dynamics of interacting bosons in homogeneous lattices in one and two dimensions", Phys. Rev. Lett. **110**, 10.1103/PhysRevLett.110.205301 (2013).

[93] L. Vidmar, S. Langer, I. P. McCulloch, U. Schneider, U. Schollwöck, and F. Heidrich-Meisner, "Sudden expansion of mott insulators in one dimension", Physical Review B - Condensed Matter and Materials Physics **88**, 10.1103/PhysRevB.88.235117 (2013).

[94] B. Neyenhuis, J. Zhang, P. W. Hess, J. Smith, A. C. Lee, P. Richerme, Z.-X. Gong, A. V. Gorshkov, and C. Monroe, "Observation of prethermalization in long-range interacting spin chains", Sci. Adv. **3**, 10.1126/sciadv.1700672 (2017).

[95] M. Mierzejewski, P. Prelovšek, and T. Prosen, "Identifying local and quasilocal conserved quantities in integrable systems", Phys. Rev. Lett. **114**, 1–7 (2015).

[96] M. Mierzejewski, J. Wronowicz, J. Pawłowski, and J. Herbrych, "Quasiballistic transport in the long-range anisotropic Heisenberg model", Phys. Rev. B **107**, 045134 (2023).

[97] R. A. Horn and C. R. Johnson, *Matrix Analysis*, 2 edition (Cambridge University Press, New York, NY, Oct. 2012).

[98] V. Simoncini and L. ELDÉN, "Krylov subspaces", The Princeton Companion to Applied Mathematics, 113–114 (2015).

[99] D. Crivelli, "Particle and energy transport in strongly driven one-dimensional quantum systems", PhD thesis (Uniwersytet Śląski w Katowicach, 2016).

[100] J. Gemmer and G. Mahler, "Distribution of local entropy in the Hilbert space of bi-partite quantum systems: origin of Jaynes' principle", Eur. Phys. J. B **31**, 249–257 (2003).

[101] S. Goldstein, J. L. Lebowitz, R. Tumulka, and N. Zanghì, "Canonical Typicality", Phys. Rev. Lett. **96**, 050403 (2006).

[102] S. Popescu, A. J. Short, and A. Winter, "Entanglement and the foundations of statistical mechanics", Nat. Phys. **2**, 754–758 (2006).

[103] A. Weisse and H. Fehske, "Exact Diagonalization Techniques", in *Computational many-particle physics*, edited by H. Fehske, R. Schneider, and A. Weisse, Lecture Notes in Physics (Springer, Berlin, Heidelberg, 2008), pp. 529–544.

[104] S. R. Garcia and R. A. Horn, *A Second Course in Linear Algebra* (Cambridge University Press, May 2017).

[105] H. Eves, *Elementary Matrix Theory* (Dover Publications, New York, Apr. 1980).

[106] V. Simoncini, "Computational Methods for Linear Matrix Equations", SIAM Rev. **58**, 377–441 (2016).

[107] J. R. Shewchuk, "An introduction to the conjugate gradient method without the agonizing pain", Science **49**, 64 (1994).

[108] C. Moler and C. Van Loan, "Nineteen Dubious Ways to Compute the Exponential of a Matrix, Twenty-Five Years Later", SIAM Rev. **45**, 3–49 (2003).

[109] P. Schmitteckert, "Nonequilibrium electron transport using the density matrix renormalization group method", Phys. Rev. B **70**, 121302 (2004).

[110] D. Stanek, C. Raas, and G. S. Uhrig, "Dynamics and decoherence in the central spin model in the low-field limit", Phys. Rev. B **88**, 155305 (2013).

[111] M. P. Zaletel, R. S. K. Mong, C. Karrasch, J. E. Moore, and F. Pollmann, "Time-evolving a matrix product state with long-ranged interactions", Phys. Rev. B **91**, 165112 (2015).

[112] P. E. Dargel, A. Wöllert, A. Honecker, I. P. McCulloch, U. Schollwöck, and T. Pruschke, "Lanczos algorithm with matrix product states for dynamical correlation functions", Phys. Rev. B **85**, 205119 (2012).

[113] N. Mohankumar and S. M. Auerbach, "On time-step bounds in unitary quantum evolution using the lanczos method", Comput. Phys. Commun. **175**, 473–481 (2006).

[114] E. Dagotto, "Correlated electrons in high-temperature superconductors", Rev. Mod. Phys. **66**, 763–840 (1994).

[115] G. D. Mahan, *Many-particle physics* (Springer US, Boston, MA, 2000).

[116] R. Steinigeweg, J. Gemmer, and W. Brenig, "Spin-current autocorrelations from single pure-state propagation", Phys. Rev. Lett. **112**, 120601 (2014).

[117] J. Sirker, R. G. Pereira, and I. Affleck, "Diffusion and Ballistic Transport in One-Dimensional Quantum Systems", Phys. Rev. Lett. **103**, 216602 (2009).

[118] R. Steinigeweg and J. Gemmer, "Density dynamics in translationally invariant spin-12 chains at high temperatures: a current-autocorrelation approach to finite time and length scales", Phys. Rev. B **80**, 184402 (2009).

[119] C. Karrasch, J. Hauschild, S. Langer, and F. Heidrich-Meisner, "Drude weight of the spin-$\frac{1}{2}$ XXZ chain: Density matrix renormalization group versus exact diagonalization", Phys. Rev. B **87**, 245128 (2013).

[120] C. Karrasch, J. H. Bardarson, and J. E. Moore, "Finite-Temperature Dynamical Density Matrix Renormalization Group and the Drude Weight of Spin-$1/2$ Chains", Phys. Rev. Lett. **108**, 227206 (2012).

[121] R. Steinigeweg, J. Gemmer, and W. Brenig, "Spin and energy currents in integrable and nonintegrable spin-1/2 chains: A typicality approach to real-time autocorrelations", Phys. Rev. B **91**, 104404 (2015).

[122] J. Richter and R. Steinigeweg, "Combining dynamical quantum typicality and numerical linked cluster expansions", Phys. Rev. B **99**, 094419 (2019).

[123] C. Bartsch and J. Gemmer, "Dynamical typicality of quantum expectation values", Phys. Rev. Lett. **102**, 8–11 (2009).

[124] R. Steinigeweg, A.Khodja, H. Niemeyer, C. Gogolin, and J. Gemmer, "Pushing the limits of the eigenstate thermalization hypothesis towards mesoscopic quantum systems", Phys. Rev. Lett. **112**, 1–5 (2014).

[125] G. S. Vitali D. Milman, *Asymptotic theory of finite dimensional normed spaces* (Springer Berlin Heidelberg, 1986).

[126] J. L. W. V. Jensen, "Sur les fonctions convexes et les inégalités entre les valeurs moyennes", Acta Math. **30**, 175–193 (1906).

[127] S. Popescu, A. J. Short, and A. Winter, *The foundations of statistical mechanics from entanglement: Individual states vs. averages*, Nov. 2006.

[128] P. Reimann, "Typicality for generalized microcanonical ensembles", Phys. Rev. Lett. **99**, 160404 (2007).

[129] J. Gemmer, M. Michel, and G. Mahler, "Quantum thermodynamics", Lect. Notes. Phys. **657**, 10.1007/b98082 (2009).

[130] F. D. M. Haldane, "Exact jastrow-gutzwiller resonating-valence-bond ground state of the spin-(1/2 antiferromagnetic heisenberg chain with 1/r2 exchange", Phys. Rev. Lett. **60**, 635–638 (1988).

[131] B. S. Shastry, "Exact solution of an s=1/2 heisenberg antiferromagnetic chain with long-ranged interactions", Phys. Rev. Lett. **60**, 639–642 (1988).

[132] M. K. Joshi, F. Kranzl, A. Schuckert, I. Lovas, C. Maier, R. Blatt, M. Knap, and C. F. Roos, "Observing emergent hydrodynamics in a long-range quantum magnet", Science **376**, 10.1126/science.abk2400 (2022).

[133] A. C. Lee, J. Smith, P. Richerme, B. Neyenhuis, P. W. Hess, J. Zhang, and C. Monroe, "Engineering large Stark shifts for control of individual clock state qubits", Physical Review A **94**, 042308 (2016).

[134] S. Langer, M. J. A. Schuetz, I. P. McCulloch, U. Schollwöck, and F. Heidrich-Meisner, "Expansion velocity of a one-dimensional, two-component fermi gas during the sudden expansion in the ballistic regime", Physical Review A - Atomic, Molecular, and Optical Physics **85**, 10.1103/PhysRevA.85.043618 (2012).

[135] P. Prelovšek, M. Mierzejewski, and J. Herbrych, "Coexistence of diffusive and ballistic transport in integrable quantum lattice models", Phys. Rev. B **104**, 1–9 (2021).

[136] P. Mazur, "Non-ergodicity of phase functions in certain systems", Physica **43**, 533–545 (1969).

[137] M. Mierzejewski, T. Prosen, and P. Prelovšek, "Approximate conservation laws in perturbed integrable lattice models", Phys. Rev. B **92**, 1–7 (2015).

[138] E. Ilievski, M. Medenjak, and T. Prosen, "Quasilocal Conserved Operators in the Isotropic Heisenberg Spin- 1/2 Chain", Phys. Rev. Lett. **115**, 120601 (2015).

[139] E. Ilievski, J. D. Nardis, B. Wouters, J.-S. Caux, F. Essler, and T. Prosen, "Complete generalized gibbs ensembles in an interacting theory", Phys. Rev. Lett. **115**, 157201 (2015).

[140] T. Prosen and E. Ilievski, "Families of quasilocal conservation laws and quantum spin transport", Phys. Rev. Lett. **111**, 057203 (2013).

[141] T. Prosen, "Quasilocal conservation laws in XXZ spin-1/2 chains: Open, periodic and twisted boundary conditions", Nucl. Phys. B **886**, 1177–1198 (2014).

[142] J. B. Conway, *A Course in Functional Analysis*, Vol. 96, Graduate Texts in Mathematics (Springer, New York, NY, 2007).

[143] L. Vidmar, B. Krajewski, J. Bonča, and M. Mierzejewski, "Phenomenology of spectral functions in disordered spin chains at infinite temperature", Phys. Rev. Lett. **127**, 230603 (2021).

[144] J. Sirker, R. G. Pereira, and I. Affleck, "Conservation laws, integrability, and transport in one-dimensional quantum systems", Phys. Rev. B **83**, 1–20 (2011).

[145] J. Sirker, "Transport in one-dimensional integrable quantum systems", SciPost Physics Lecture Notes **17**, 1–19 (2020).

[146] F. Göhmann, K. Kozlowski, J. Sirker, and J. Suzuki, "Spin conductivity of the XXZ chain in the antiferromagnetic massive regime", SciPost Physics **12**, 1–28 (2022).

[147] F. W. Byron and R. W. Fuller, *Mathematics of Classical and Quantum Physics*, Vol. 24, t. 1-2 (Dover Publications, 1992), pp. 52–53.

A

Hilbert subspaces with fixed momentum

B

Optical conductivity in spin chains

Sirker et al. [144] and Sirker [145] for derivation of $\sigma(\omega)$ from Kubro formula Göhmann et al. [146] for the derivation of Kubo formula

C

Two Fourier transforms

The goal of this appending is the calculation of two Fourier transforms, which appear in the main text. They originate from the definition of finite-time averaging (4.7) and the integrated spectral function (4.22). Let us begin with the latter one, as it is simpler. We have

$$\begin{aligned}
\mathcal{F}\left[(A(t)|B)\right] &= \lim_{\varepsilon\to 0^+}\frac{1}{2\pi}\int_{-\infty}^{\infty}\mathrm{d}t\; e^{i\omega t-|t|\varepsilon}\,(A(t)|B) = \lim_{\varepsilon\to 0^+}\frac{1}{2\pi}\int_{-\infty}^{\infty}\mathrm{d}t\; e^{i\omega t-|t|\varepsilon}\frac{1}{\mathcal{D}}\,\mathrm{Tr}\left[\left(e^{iHt}Ae^{-iHt}\right)^{\dagger}B\right] \\
&= \lim_{\varepsilon\to 0^+}\frac{1}{2\pi}\int_{-\infty}^{\infty}\mathrm{d}t\; e^{i\omega t-|t|\varepsilon}\frac{1}{\mathcal{D}}\,\mathrm{Tr}\left[e^{iHt}\left(\sum_m |m\rangle\langle m|\right)A\left(\sum_n |n\rangle\langle n|\right)e^{-iHt}B\right] \\
&= \frac{1}{\mathcal{D}}\frac{1}{2\pi}\sum_{n,m}\lim_{\varepsilon\to 0^+}\int_{-\infty}^{\infty}\mathrm{d}t\; e^{i\omega t-|t|\varepsilon}\,\mathrm{Tr}\left[e^{i\epsilon_m t}\,|m\rangle\langle m|\,A\,|n\rangle\langle n|\,e^{-i\epsilon_n t}B\right] \\
&= \frac{1}{\mathcal{D}}\frac{1}{2\pi}\sum_{n,m}A_{mn}\lim_{\varepsilon\to 0^+}\int_{-\infty}^{\infty}\mathrm{d}t\; e^{i\omega t-|t|\varepsilon}e^{i(\epsilon_m-\epsilon_n)t}\sum_k\underbrace{\langle k|m\rangle}_{=\delta_{km}}\langle n|B|k\rangle \\
&= \frac{1}{\mathcal{D}}\frac{1}{2\pi}\sum_{n,m}A_{mn}B_{nm}\underbrace{\lim_{\varepsilon\to 0^+}\int_{-\infty}^{\infty}\mathrm{d}t\; e^{i\omega t-|t|\varepsilon}e^{i(\epsilon_m-\epsilon_n)t}}_{\mathcal{I}}
\end{aligned} \tag{C.1}$$

Let us massage it a bit further, by calculating the integral $\mathcal{I}$ explicitly.

$$\begin{aligned}
\mathcal{I} &= \lim_{\varepsilon\to 0^+}\int_{-\infty}^{\infty}\mathrm{d}t\; e^{i(\epsilon_m-\epsilon_n+\omega)t-|t|\varepsilon} = \lim_{\varepsilon\to 0^+}\left[\lim_{T_1\to-\infty}\int_{T_1}^{0}\mathrm{d}t\; e^{i(\epsilon_m-\epsilon_n+\omega-i\varepsilon)t}\right. \\
&\left.+\lim_{T_2\to\infty}\int_0^{T_2}\mathrm{d}t\; e^{i(\epsilon_m-\epsilon_n+\omega+i\varepsilon)t}\right] = \lim_{\varepsilon\to 0^+}\left[\lim_{T_1\to-\infty}\frac{1-e^{i(\epsilon_m-\epsilon_n+\omega)T_1}e^{\varepsilon T_1}}{i(\epsilon_m-\epsilon_n+\omega-i\varepsilon)}\right. \\
&\left.+\lim_{T_2\to\infty}\frac{e^{i(\epsilon_m-\epsilon_n+\omega)T_2}e^{-\varepsilon T_2}-1}{i(\epsilon_m-\epsilon_n+\omega+i\varepsilon)}\right] = \lim_{\varepsilon\to 0^+}\left[\frac{i}{\epsilon_n-\epsilon_m-\omega+i\varepsilon}+\frac{i}{\epsilon_m-\epsilon_n+\omega+i\varepsilon}\right] \\
&= \lim_{\varepsilon\to 0^+}\frac{2\varepsilon}{(\epsilon_m-\epsilon_n+\omega-i\varepsilon)(\epsilon_m-\epsilon_n+\omega+i\varepsilon)} = \lim_{\varepsilon\to 0^+}\frac{2\varepsilon}{(\epsilon_m-\epsilon_n+\omega)^2+\varepsilon^2}
\end{aligned} \tag{C.2}$$

The obtained result is a limit of the so-called Poisson kernel. This happens to be a representation of Dirac δ in the form of a limit of a sequence of functions [147]

$$\lim_{\varepsilon\to 0^+}\frac{1}{\pi}\frac{\varepsilon}{x^2+\varepsilon^2} = \delta(x) \tag{C.3}$$

Thus we get

$$\mathcal{I} = \lim_{\varepsilon \to 0^+} \frac{2\varepsilon}{(\epsilon_m - \epsilon_n + \omega)^2 + \varepsilon^2} = 2\pi\delta(\epsilon_m - \epsilon_n + \omega) \tag{C.4}$$

Inserting this result into equation (C.1) we arrive at

$$\begin{aligned} \mathcal{F}\left[(A(t)|B)\right] = &\frac{1}{\mathcal{D}} \frac{1}{2\pi} \sum_{n,m} A_{mn} B_{nm} \lim_{\varepsilon \to 0^+} \int_{-\infty}^{\infty} \mathrm{d}t \; e^{i\omega t - |t|\varepsilon} e^{i(\epsilon_m - \epsilon_n)t} \\ = &\frac{1}{\mathcal{D}} \sum_{n,m} A_{mn} B_{nm} \delta(\epsilon_m - \epsilon_n + \Omega) \end{aligned} \tag{C.5}$$

which is our desired results.